

Improved FFT-based Homogenization for Periodic Media

J. Vondřejc*

September 5, 2018

Abstract

Moulinec and Suquet introduced FFT-based homogenization in 1994, and twenty years later, their approach is still effective for evaluating the homogenized properties arising from the periodic cell problem. This paper builds on the author's (2013) variational reformulation approximated by trigonometric polynomials establishing two numerical schemes: Galerkin approximation (Ga) and a version with numerical integration (GaNi). The latter approach, fully equivalent to the original Moulinec-Suquet algorithm, was used to evaluate guaranteed upper-lower bounds on homogenized coefficients incorporating a closed-form double grid quadrature. Here, these concepts are employed for the Ga scheme. Despite Ga's higher computational requirements, it outperforms GaNi with improved guaranteed bounds together with more predictable and monotone behaviors for an increase in the number of grid points. Numerical integration heading to block-sparse linear systems is extended here to materials defined via high-resolution images in a way which allows for effective treatment using the FFT algorithm. Shifts in FFT result in a reduction to the original grid. Minimization of the bounds during iterations of conjugate gradients is effective, particularly when incorporating a solution from a coarser grid. The methodology presented here for the scalar linear elliptic problem could be extended to more complex frameworks.

Keywords: Guaranteed bounds; Variational methods; Numerical homogenization; Galerkin approximation; Trigonometric polynomials; Fourier Transform

1 Introduction

This paper is devoted to FFT-based homogenization, a numerical method for evaluating homogenized (effective) material coefficients which are essential in multiscale design. This method, which is an alternative to Finite Differences [1, 2], Finite Elements [3, 4], Boundary Elements [5, 6], or Fast Multipole Methods [7, 8], enables the direct treatment of material coefficients defined via high-resolution images. The drawback of low adaptability originating from the use of regular discretization grids is offset by easy implementation when compared to conventional FEM (Finite Element Method) and because of the algorithm's effectiveness arising from the FFT (fast Fourier transform) used in linear iterative solvers. Moreover, because the same structure is observed for both primal and the dual formulations, FFT-based homogenization enables straightforward evaluation of guaranteed upper-lower bounds on homogenized properties [9]. This ensures the method's reliability.

This paper generalizes a double grid numerical integration to FFT-based homogenization [21, 9] leading to an improved algorithm with significantly tighter guaranteed bounds on homogenized coefficients when compared to the original method [18]. For simplicity and clarity, the approach is presented here only for a scalar linear elliptic problem describing stationary heat transfer, electric conductivity, or diffusion. However, the improved method could be generalized to more

*New Technologies for the Information Society, Faculty of Applied Sciences, University of West Bohemia, Univerzitní 2732/8, 306 14 Plzeň, Czech Republic. E-mail: vondrejcz@gmail.com

complex problems such as large deformations [10], viscoelasticity [11], thermo-elasticity [12], or fracture and damage mechanics [13, 14].

Section 1.1 describes the evaluation of effective properties as a result of the homogenization process. Section 1.2 provides a detailed overview of FFT-based homogenization schemes, and section 1.3 shows its application to obtain guaranteed bounds on the homogenized properties. Section 1.4 describes the structure of the paper.

1.1 Periodic cell problem

The model problem consists of an evaluation of homogenized properties $\mathbf{A}_H \in \mathbb{R}^{d \times d}$ that comply with the minimization problem

$$(\mathbf{A}_H \mathbf{E}, \mathbf{E})_{\mathbb{R}^d} = \inf_{u \in H_{\#, (0)}^1(\mathcal{Y})} \frac{1}{|\mathcal{Y}|} \int_{\mathcal{Y}} (\mathbf{A}(\mathbf{x})[\mathbf{E} + \nabla u(\mathbf{x})], [\mathbf{E} + \nabla u(\mathbf{x})])_{\mathbb{R}^d} d\mathbf{x} \quad (1a)$$

for arbitrary vector $\mathbf{E} \in \mathbb{R}^d$. The region $\mathcal{Y} = \prod_{\alpha=1}^d (-\frac{Y_\alpha}{2}, \frac{Y_\alpha}{2}) \subset \mathbb{R}^d$ accounts for a d -dimensional cell representing a periodic material defined through the bounded, symmetric, and uniformly elliptic \mathcal{Y} -periodic matrix function $\mathbf{A} : \mathbb{R}^d \rightarrow \mathbb{R}^{d \times d}$. The trial space $H_{\#, (0)}^1(\mathcal{Y})$, consisting of the \mathcal{Y} -periodic scalar functions $u : \mathcal{Y} \rightarrow \mathbb{R}$ with a square integrable gradient and zero mean, includes minimizers $u^{(\mathbf{E})}$ satisfying stationary equations for a particular $\mathbf{E} \in \mathbb{R}^d$:

$$\int_{\mathcal{Y}} (\mathbf{A}(\mathbf{x}) \nabla u^{(\mathbf{E})}(\mathbf{x}), \nabla v(\mathbf{x}))_{\mathbb{R}^d} d\mathbf{x} = - \int_{\mathcal{Y}} (\mathbf{A}(\mathbf{x}) \mathbf{E}, \nabla v(\mathbf{x}))_{\mathbb{R}^d} d\mathbf{x} \quad \forall v \in H_{\#, (0)}^1(\mathcal{Y}). \quad (1b)$$

Originally, the macroscopic problem (1a) introducing homogenized coefficients arises as a result of the well-established homogenization process [15, 16, 17]. It deals with a ε -parametrized scalar elliptic equation

$$\int_{\Omega} (\mathbf{A}^\varepsilon(\tilde{\mathbf{x}}) \nabla u^\varepsilon(\tilde{\mathbf{x}}), \nabla v(\tilde{\mathbf{x}}))_{\mathbb{R}^d} d\tilde{\mathbf{x}} = F(v) \quad \forall v \in H_0^1(\Omega) \quad (2)$$

for a scalar quantity $u^\varepsilon : \Omega \rightarrow \mathbb{R}$ from the Sobolev space $H_0^1(\Omega)$ — the space of functions which has a square integrable gradient and zero trace on the boundary of Ω . The positive parameter $\varepsilon > 0$ determines the size of the cell $\varepsilon\mathcal{Y}$ which periodically fills the whole region $\Omega \subset \mathbb{R}^d$ and also determines $\varepsilon\mathcal{Y}$ -periodic material coefficients $\mathbf{A}^\varepsilon : \Omega \rightarrow \mathbb{R}^{d \times d}$ associated with those in (1a) via

$$\mathbf{A}^\varepsilon(\tilde{\mathbf{x}}) = \mathbf{A}\left(\frac{\tilde{\mathbf{x}}}{\varepsilon}\right) \text{ for } \tilde{\mathbf{x}} \in \Omega$$

and which oscillates more the smaller the microstructure parameter ε is. The linear functional $F : H_0^1(\Omega) \rightarrow \mathbb{R}$, possibly ε -dependent, covers both the prescribed sources and the various boundary conditions.

The direct solution of (2) by standard numerical methods, although theoretically possible, is unfeasible for small parameters ε due to the computational demands arising from highly oscillating solutions. Alternatively, the complexity of the problem (2) can be reduced with homogenization providing a limit process for $\varepsilon \rightarrow 0$. The former problem (2) is then replaced with the homogenized formulation

$$\int_{\Omega} \mathbf{A}_H \nabla u_H(\tilde{\mathbf{x}}) \cdot \nabla v(\tilde{\mathbf{x}}) d\tilde{\mathbf{x}} = F(v) \quad \forall v \in H_0^1(\Omega),$$

where the constant material $\mathbf{A}_H \in \mathbb{R}^{d \times d}$, independent of the spatial variable, is defined by our model problem (1a). The averaged solution u_H lacks the oscillating part; nevertheless, according to the so-called corrector result, the original solution u^ε of (2) is recoverable using corrector functions obtained as minimizers of (1a).

1.2 FFT-based Homogenization

This section is dedicated to a numerical solution of the cell problem (1) using the FFT-based method introduced in 1994 by Moulinec and Suquet [18] as a new method. Nevertheless, the theories regarding this method, including discretization and convergence of approximate solutions, have been provided only recently.

Brisard and Dormieux in [19, 20] described the method using Galerkin approximation with piece-wise constant basis functions using a Lippmann-Schwinger integral equation. This formulation employs the Green function derived for a reference medium as a parameter of the method, influencing both the quality of the approximate solutions and the convergence of linear solvers.

In this paper, FFT-based methods build upon a variational reformulation by the author and co-workers [21, 22, 23]. Thus, the reference medium parameter is naturally avoided and two discretization schemes to the cell problem (1) studied in [22, sections 4.2 and 4.3] are revealed: Galerkin approximation (Ga)

$$(\mathbf{A}_{\text{H},N} \mathbf{E}, \mathbf{E})_{\mathbb{R}^d} = \inf_{u_N \in \mathcal{T}_N} \int_{\mathcal{Y}} (\mathbf{A}(\mathbf{x})[\mathbf{E} + \nabla u_N(\mathbf{x})], \mathbf{E} + \nabla u_N(\mathbf{x}))_{\mathbb{R}^d} d\mathbf{x}, \quad (3a)$$

and Galerkin approximation with numerical integration (GaNi)

$$(\tilde{\mathbf{A}}_{\text{H},N}^{\text{GaNi}} \mathbf{E}, \mathbf{E})_{\mathbb{R}^d} = \inf_{u_N \in \mathcal{T}_N} \int_{\mathcal{Y}} (\mathcal{Q}_N[\mathbf{A}(\mathbf{E} + \nabla u_N)](\mathbf{x}), \mathbf{E} + \nabla u_N(\mathbf{x}))_{\mathbb{R}^d} d\mathbf{x}, \quad (3b)$$

which is performed with the interpolation operator \mathcal{Q}_N (see (59) for the definition), providing a trapezoidal rule. An approximation is carried out with a truncated Fourier series space

$$\mathcal{T}_N = \left\{ \sum_{\mathbf{k} \in \mathbb{Z}_N^d \setminus \{\mathbf{0}\}} c^{\mathbf{k}} \varphi_{\mathbf{k}} : c^{\mathbf{k}} = \overline{c^{-\mathbf{k}}} \in \mathbb{C} \right\} \quad \text{for } \mathbb{Z}_N^d = \left\{ \mathbf{k} \in \mathbb{Z}^d : -\frac{N_\alpha}{2} < k_\alpha < \frac{N_\alpha}{2} \right\}$$

and for Fourier basis functions $\varphi_{\mathbf{k}}(\mathbf{x}) = \exp(2\pi i \sum_{\alpha=1}^d \frac{k_\alpha x_\alpha}{Y_\alpha})$ having bounded frequencies $\mathbf{k} \in \mathbb{Z}_N^d$.

The discretization of the cell problem (1) with trigonometric polynomials is a standard approach which was used, for example, in [24, 25, 26, 27]. However, its connection to FFT-based homogenization methods [18], according to the best of my knowledge, was established only recently in [28], drawing inspiration from a trigonometric collocation method for the Lippmann-Schwinger equation, [29] and [30, sections 8–10]. Thus, the original Moulinec-Suquet scheme [18, 31] is interpreted using the Galerkin method (3b) with a trapezoidal numerical integration by the author et al. [23] and [22, section 5.2]. Although, contrary to the equations here (1) and (3), the standard FFT-based method is formulated for gradient field $\mathbf{e} = \nabla u : \mathcal{Y} \rightarrow \mathbb{R}^d$ or for strains instead of displacements in linear elasticity; the equivalence of both formulations is discussed later in Remark 11.

While the numerical treatment of the GaNi scheme (3b) relies on the regularity of material coefficients \mathbf{A} , the Ga (3a) requires knowledge about the Fourier coefficients of \mathbf{A} . The exact numerical integration to (3a) leading to the fully populated matrix, employed e.g. in [24, 25], can be improved by a double grid quadrature introduced by the author in [21, 9]. The fully discrete formulation then constitutes the same block-sparse structure as the GaNi scheme (3b).

Apart from the theoretically supported formulations in (3) and the Brisard and Dormieux approach [19, 20] both heading to FFT-based schemes, there are various other modifications and improvements. Bonnet, in [32], incorporated the so-called shape functions in Fourier space to enhance the performance and accuracy of the method. Later, in [33], the authors provided a polarization-based scheme which can handle arbitrary phase contrast (voids and stiff inclusions); this can be also managed by a numerical method based on augmented Lagrangians [34]. Recently,

Willot et al. in [35] adjusted the integral kernel in the Lippmann-Schwinger equation which led to improved accuracy in approximate solutions, illustrated with a comparison using an analytical solution [36]. Significant attention was granted to improving the linear solvers leading to the accelerated schemes [37, 12] or the application of conjugate gradient method [28, 19].

1.3 Guaranteed bounds on homogenized properties

The theory of guaranteed bounds on homogenized coefficients has been the subject of many studies in analytical homogenization theories. These techniques employ the primal-dual formulations of the cell problem (1) with limited — and often uncertain — information about the material coefficients \mathbf{A} . Specific examples include the Voigt [38], Reuss [39], and Hashin-Shtrikman bounds [40]; see the monographs [24, 41, 42, 43, 44] for a more complete overview. Because the bounds rely on limited data, their performance rapidly deteriorates for highly-contrasted media.

Relatively less attention has been given to the computable upper-lower bounds arising from a conforming approximation to the cell problem (1). These bounds can be made arbitrarily accurate if the approximate solutions converge to the solution of the cell problem (1). Moreover, the bounds are guaranteed if they allow for closed-form evaluation. Dvořák and Haslinger, to our knowledge, specified the relevant ideas in their pioneering work [45, 46], which applied the approach to the p -version of FEM. The application to the h -version of FEM occurs in [47] and to Fourier discretization in [24, 25].

The effective evaluation of upper-lower bounds using FFT has been provided recently in [48] for linear elasticity and later in [49] for permeability. Both frameworks rely on the Hashin-Shtrikman functional or the Lippmann-Schwinger equation, respectively, discretized with the Brisard–Dormieux method [20] assuming piecewise-constant approximations. However, the evaluation of bounds is based on the summation of an infinite series leading to the loss of guarantee.

The approximation with trigonometric polynomials used here in (3) and in [24, 25] provide guaranteed bounds. According to [9] and section 4 in this paper, this approach enables effective closed-form evaluation for material properties that have an analytical expression of Fourier coefficients. Because this class is sufficiently large, allowing for approximation of material coefficients presented in section 4.5, this drawback is insignificant.

Now, the author will discuss the concepts leading to the guaranteed bounds on homogenized properties used in this paper. Initially, in the author’s previous work [9], the approximate minimizers $u_{\mathbf{N}}^{\text{GaNi},(\mathbf{E})}$ of the GaNi scheme (3b) were a posteriori used to evaluate the homogenized matrix $\tilde{\mathbf{A}}_{\mathbf{H},\mathbf{N}} \in \mathbb{R}^{d \times d}$ satisfying

$$\left(\tilde{\mathbf{A}}_{\mathbf{H},\mathbf{N}}\mathbf{E}, \mathbf{E}\right)_{\mathbb{R}^d} = \left(\mathbf{A}(\mathbf{E} + \nabla u_{\mathbf{N}}^{\text{GaNi},(\mathbf{E})}), \mathbf{E} + \nabla u_{\mathbf{N}}^{\text{GaNi},(\mathbf{E})}\right)_{L^2_{\#}(\mathcal{Y};\mathbb{R}^d)} \quad (4)$$

for all $\mathbf{E} \in \mathbb{R}^d$. When the homogenized coefficients defined in (1a), (3a), and (4) provide a guaranteed upper-bound structure on the homogenized coefficients satisfying

$$\left(\mathbf{A}_{\mathbf{H}}\mathbf{E}, \mathbf{E}\right)_{\mathbb{R}^d} \leq \left(\mathbf{A}_{\mathbf{H},\mathbf{N}}\mathbf{E}, \mathbf{E}\right)_{\mathbb{R}^d} \leq \left(\tilde{\mathbf{A}}_{\mathbf{H},\mathbf{N}}\mathbf{E}, \mathbf{E}\right)_{\mathbb{R}^d} \quad \forall \mathbf{E} \in \mathbb{R}^d,$$

the effective properties from the Ga scheme (3a) outperform those of the GaNi scheme (4). This structure is based on the following inequalities

$$\begin{aligned} \inf_{u \in H^1_{\#, (0)}(\mathcal{Y})} \left(\mathbf{A}(\mathbf{E} + \nabla u), \mathbf{E} + \nabla u\right)_{L^2_{\#}(\mathcal{Y};\mathbb{R}^d)} &\leq \inf_{u_{\mathbf{N}} \in \mathcal{T}_{\mathbf{N}}} \left(\mathbf{A}(\mathbf{E} + \nabla u_{\mathbf{N}}), \mathbf{E} + \nabla u_{\mathbf{N}}\right)_{L^2_{\#}(\mathcal{Y};\mathbb{R}^d)} \\ &\leq \left(\mathbf{A}(\mathbf{E} + \nabla u_{\mathbf{N}}^{\text{GaNi},(\mathbf{E})}), \mathbf{E} + \nabla u_{\mathbf{N}}^{\text{GaNi},(\mathbf{E})}\right)_{L^2_{\#}(\mathcal{Y};\mathbb{R}^d)} \end{aligned}$$

which hold as a result of the conforming approximation $u_{\mathbf{N}}^{\text{GaNi},(\mathbf{E})} \in \mathcal{T}_{\mathbf{N}} \subset H^1_{\#, (0)}(\mathcal{Y})$. The dual formulation then produces the guaranteed lower bounds described in detail in section 3.4.

The author also emphasizes that the homogenized coefficients $\tilde{\mathbf{A}}_{\mathbf{H},\mathbf{N}}^{\text{GaNi}}$ of the GaNi formulation (3b) are indifferent to the bounds because they can over- or underestimate them [9, Figure 9]. Moreover, these bounds can be made arbitrarily accurate thanks to the convergence analysis of approximate solutions provided by Vondřejc et al. [21, 22] and improved by Schneider [50] to account for rough coefficients.

The guaranteed bounds incorporating trigonometric polynomials were mostly calculated with the Hashin-Shtrikman functional [24]. The exceptional work [25] equivalent to (3a) is improved here by incorporating the FFT algorithm and by using a double grid quadrature, which leads to a sparse structure according to [21, 9]. In [51], these ideas have been applied to linear elasticity illustrating that the classical variational formulation used here is always better than the Hashin-Shtrikman formulation.

1.4 Content of the paper

This paper is organized as follows. Notation and preliminaries to the periodic functions, Fourier transform, and Helmholtz decomposition presented in section 2 are followed in section 3 with the continuous homogenization problem. Using the results regarding trigonometric polynomials in appendix A, section 3 also contains a description of discretization using Galerkin methods for both primal and dual formulations leading to guaranteed bounds on homogenized coefficients. The methodology for evaluating guaranteed bounds (3a) and (4) is presented in section 4. Particularly in section 4.3, the double grid quadrature from [9] is generalized for materials defined via high-resolution images. In section 4.4, the numerical scheme on the double grid is reduced to the original grid using shifts of DFT (58). In section 4.5, the material properties without analytical expression of Fourier coefficients are approximated in a way to still obtain the guaranteed bounds on the homogenized properties. Then a numerical treatment is presented in section 5 for fully discrete formulations, including the resolution of minimizers from linear systems. Numerical examples in section 6 confirm the theoretical results and provide a numerical comparison between the Ga (3a) and GaNi schemes (3b) corresponding to the original Moulinec-Suquet algorithm.

2 Notation and preliminaries

In the sections 2.1 and 2.2, the author introduces notation and recalls some useful facts related to matrix analysis and to spaces of periodic functions and the Fourier transform. Section 2.3 is dedicated to the Helmholtz decomposition of vector-valued periodic functions and its description with orthogonal projections, essential for the duality arguments in both discrete and continuous settings.

2.1 Vectors and matrices

In the subsequent section, d is reserved for the dimension of the model problem, assuming $d = 2, 3$. To keep the notation compact, \mathbb{X} abbreviates the space of scalars, vectors, or matrices, i.e. \mathbb{R}, \mathbb{R}^d , or $\mathbb{R}^{d \times d}$, and $\hat{\mathbb{X}}$ is used for their complex counterparts, i.e. \mathbb{C}, \mathbb{C}^d , or $\mathbb{C}^{d \times d}$. Vectors and matrices are denoted by boldface letters, e.g. $\mathbf{u}, \mathbf{v} \in \mathbb{R}^d$ or $\mathbf{M} \in \mathbb{R}^{d \times d}$, with Greek letters used when referring to their entries; e.g. $\mathbf{M} = (M_{\alpha\beta})_{\alpha,\beta=1,\dots,d}$. Matrix $\mathbf{I} = (\delta_{\alpha\beta})_{\alpha\beta}$ denotes the identity matrix whereas the symbol $\delta_{\alpha\beta}$ is reserved for the Kronecker delta, defined as $\delta_{\alpha\beta} = 1$ for $\alpha = \beta$ and $\delta_{\alpha\beta} = 0$ otherwise.

As usual, the matrix-vector product $\mathbf{M}\mathbf{v}$, the matrix-matrix product $\mathbf{M}\mathbf{L}$, and the outer

product $\mathbf{u} \otimes \mathbf{v}$ refer to

$$(\mathbf{M}\mathbf{u})_\alpha = \sum_\beta M_{\alpha\beta}u_\beta, \quad (\mathbf{M}\mathbf{L})_{\alpha\beta} = \sum_\gamma M_{\alpha\gamma}L_{\gamma\beta}, \quad (\mathbf{u} \otimes \mathbf{v})_{\alpha\beta} = u_\alpha v_\beta,$$

where the author assumes that α and β range from 1 to d for the sake of brevity. Moreover, the spaces are endowed with the following inner product and norms, e.g.

$$(\mathbf{u}, \mathbf{v})_{\mathbb{C}^d} = \sum_\alpha u_\alpha \overline{v_\alpha}, \quad \|\mathbf{u}\|_{\mathbb{C}^d}^2 = (\mathbf{u}, \mathbf{u})_{\mathbb{C}^d}, \quad \|\mathbf{M}\|_{\mathbb{C}^{d \times d}} = \max_{\mathbf{u} \neq \mathbf{0}} \frac{\|\mathbf{M}\mathbf{u}\|_{\mathbb{C}^d}}{\|\mathbf{u}\|_{\mathbb{C}^d}}. \quad (5)$$

The set $\mathbb{R}_{\text{spd}}^{d \times d} \subset \mathbb{R}^{d \times d}$ denotes the space of symmetric positive definite matrices satisfying

$$M_{\alpha\beta} = M_{\beta\alpha} \quad \text{for all } \alpha, \beta, \quad (\mathbf{M}\mathbf{u}, \mathbf{u})_{\mathbb{R}^d} > 0 \quad \text{for all } \mathbf{u} \in \mathbb{R}^d \text{ such that } \mathbf{u} \neq \mathbf{0}.$$

In this space, the trace operator, $\text{tr } \mathbf{M} = \sum_\alpha M_{\alpha\alpha}$ for $\mathbf{M} \in \mathbb{R}^{d \times d}$, becomes an equivalent norm to (5) since it equals the sum of eigenvalues, cf. [52, section 5.6]. The Löwner partial order, cf. [52, section 7.7], of symmetric positive definite matrices turns out to be useful, i.e. for $\mathbf{L}, \mathbf{M} \in \mathbb{R}_{\text{spd}}^{d \times d}$, the author writes

$$\mathbf{L} \preceq \mathbf{M} \quad \text{if} \quad (\mathbf{L}\mathbf{u}, \mathbf{u})_{\mathbb{R}^d} \leq (\mathbf{M}\mathbf{u}, \mathbf{u})_{\mathbb{R}^d} \quad \text{for all } \mathbf{u} \in \mathbb{R}^d.$$

The inverse inequality property will be also systematically used

$$\mathbf{L} \preceq \mathbf{M} \quad \iff \quad \mathbf{M}^{-1} \preceq \mathbf{L}^{-1} \quad (6)$$

for $\mathbf{L}, \mathbf{M} \in \mathbb{R}_{\text{spd}}^{d \times d}$, cf. [52, Corollary 7.7.4.(a)].

2.2 Periodic functions and Fourier transform

The author considers cells in the form $\mathcal{Y} = \prod_\alpha (-\frac{Y_\alpha}{2}, \frac{Y_\alpha}{2})$ for $\mathbf{Y} \in \mathbb{R}^d$ such that $Y_\alpha > 0$. Then, a function $\mathbf{f} : \mathbb{R}^d \rightarrow \mathbb{X}$ is \mathcal{Y} -periodic if

$$\mathbf{f}(\mathbf{x} + \sum_\alpha Y_\alpha \mathbf{k}_\alpha) = \mathbf{f}(\mathbf{x}) \quad \text{for all } \mathbf{x} \in \mathcal{Y} \text{ and all } \mathbf{k} \in \mathbb{Z}^d.$$

The space $C_{\#}(\mathcal{Y}; \mathbb{X})$ collects all continuous \mathcal{Y} -periodic functions $\mathbb{R}^d \rightarrow \mathbb{X}$. For $p \in \{2, \infty\}$,

$$L_{\#}^p(\mathcal{Y}; \mathbb{X}) = \left\{ \mathbf{f} : \mathcal{Y} \rightarrow \mathbb{X} : \mathbf{f} \text{ is } \mathcal{Y}\text{-periodic, measurable, and } \|\mathbf{f}\|_{L_{\#}^p(\mathcal{Y}; \mathbb{X})} < \infty \right\}$$

denotes the Lebesgue space equipped with the norm

$$\|\mathbf{f}\|_{L_{\#}^p(\mathcal{Y}; \mathbb{X})} = \begin{cases} \text{ess sup}_{\mathbf{x} \in \mathcal{Y}} \|\mathbf{f}(\mathbf{x})\|_{\mathbb{X}} & \text{for } p = \infty, \\ \left(|\mathcal{Y}|^{-1} \int_{\mathcal{Y}} \|\mathbf{f}(\mathbf{x})\|_{\mathbb{X}}^2 d\mathbf{x} \right)^{1/2} & \text{for } p = 2. \end{cases}$$

where $|\mathcal{Y}| = \prod_\alpha Y_\alpha$ denotes the Lebesgue measure of the cell \mathcal{Y} .

For the sake of brevity, the author writes $L_{\#}^p(\mathcal{Y})$ instead of $L_{\#}^p(\mathcal{Y}; \mathbb{R})$, and often shortens $L_{\#}^2(\mathcal{Y}; \mathbb{R}^d)$ to $L_{\#}^2$ when referring to the norms and the inner product.

The Fourier transform of $\mathbf{f} \in L_{\#}^2(\mathcal{Y}; \mathbb{X})$ is denoted by

$$\widehat{\mathbf{f}}(\mathbf{k}) = \overline{\widehat{\mathbf{f}}(-\mathbf{k})} = \frac{1}{|\mathcal{Y}|} \int_{\mathcal{Y}} \mathbf{f}(\mathbf{x}) \varphi_{-\mathbf{k}}(\mathbf{x}) d\mathbf{x} \in \widehat{\mathbb{X}} \quad \text{for } \mathbf{k} \in \mathbb{Z}^d, \quad (7)$$

where the Fourier trigonometric polynomials,

$$\varphi_{\mathbf{k}}(\mathbf{x}) = \exp\left(2\pi i(\boldsymbol{\xi}(\mathbf{k}), \mathbf{x})_{\mathbb{R}^d}\right) \quad \text{for } \mathbf{x} \in \mathcal{Y} \text{ and } \mathbf{k} \in \mathbb{Z}^d \quad (8)$$

with $\boldsymbol{\xi}(\mathbf{k}) = (k_\alpha/Y_\alpha)_\alpha$, forming an orthonormal basis $\{\varphi_{\mathbf{k}}\}_{\mathbf{k} \in \mathbb{Z}^d}$ of $L^2_{\#}(\mathcal{Y})$, i.e.

$$(\varphi_{\mathbf{k}}, \varphi_{\mathbf{m}})_{L^2_{\#}(\mathcal{Y})} = \delta_{\mathbf{k}\mathbf{m}} \quad \text{for } \mathbf{k}, \mathbf{m} \in \mathbb{Z}^d, \quad (9)$$

cf. [53, pp. 89–91]. Thus, every function $\mathbf{f} \in L^2_{\#}(\mathcal{Y}; \mathbb{X})$ can be expressed in the form

$$\mathbf{f}(\mathbf{x}) = \sum_{\mathbf{k} \in \mathbb{Z}^d} \widehat{\mathbf{f}}(\mathbf{k}) \varphi_{\mathbf{k}}(\mathbf{x}) \quad \text{for } \mathbf{x} \in \mathcal{Y}.$$

The space $L^2_{\#}(\mathcal{Y}; \mathbb{R}^d)$ is also a Hilbert space with an inner product

$$(\mathbf{u}, \mathbf{v})_{L^2_{\#}(\mathcal{Y}; \mathbb{R}^d)} = \frac{1}{|\mathcal{Y}|} \int_{\mathcal{Y}} (\mathbf{u}(\mathbf{x}), \mathbf{v}(\mathbf{x}))_{\mathbb{R}^d} d\mathbf{x} = \sum_{\mathbf{k} \in \mathbb{Z}^d} (\widehat{\mathbf{u}}(\mathbf{k}), \widehat{\mathbf{v}}(\mathbf{k}))_{\mathbb{C}^d}, \quad (10)$$

which can be expressed, thanks to Parseval's theorem, in both the original and Fourier spaces.

The mean value of function $\mathbf{f} \in L^2_{\#}(\mathcal{Y}; \mathbb{X})$ over periodic cell \mathcal{Y} is denoted as

$$\langle \mathbf{f} \rangle = \frac{1}{|\mathcal{Y}|} \int_{\mathcal{Y}} \mathbf{f}(\mathbf{x}) d\mathbf{x} = \widehat{\mathbf{f}}(\mathbf{0}) \in \mathbb{X}$$

and corresponds to the zero-frequency Fourier coefficient.

2.3 Helmholtz decomposition for periodic functions

Operator \oplus denotes the direct sum of mutually orthogonal subspaces, e.g. $\mathbb{R}^d = \mathbf{U}^{(1)} \oplus \mathbf{U}^{(2)} \oplus \dots \oplus \mathbf{U}^{(d)}$ for vectors $\mathbf{U}^{(\alpha)} = (\delta_{\alpha\beta})_\beta$. According to the Helmholtz decomposition [16, pages 6–7], $L^2_{\#}(\mathcal{Y}; \mathbb{R}^d)$ admits an orthogonal decomposition

$$L^2_{\#}(\mathcal{Y}; \mathbb{R}^d) = \mathcal{U} \oplus \mathcal{E} \oplus \mathcal{J} \quad (11)$$

into the subspaces of constant, zero-mean curl-free, and zero-mean divergence free fields

$$\mathcal{U} = \{\mathbf{v} \in L^2_{\#}(\mathcal{Y}; \mathbb{R}^d) : \mathbf{v}(\mathbf{x}) = \langle \mathbf{v} \rangle \text{ for all } \mathbf{x} \in \mathcal{Y}\}, \quad (12a)$$

$$\mathcal{E} = \{\mathbf{v} \in L^2_{\#}(\mathcal{Y}; \mathbb{R}^d) : \text{curl } \mathbf{v} = \mathbf{0}, \langle \mathbf{v} \rangle = \mathbf{0}\}, \quad (12b)$$

$$\mathcal{J} = \{\mathbf{v} \in L^2_{\#}(\mathcal{Y}; \mathbb{R}^d) : \text{div } \mathbf{v} = 0, \langle \mathbf{v} \rangle = \mathbf{0}\}. \quad (12c)$$

Here, the differential operators curl and div are understood in the Fourier sense, so that

$$(\text{curl } \mathbf{u})_{\alpha\beta} = \sum_{\mathbf{k} \in \mathbb{Z}^d} 2\pi i (\xi_\beta(\mathbf{k}) \widehat{u}_\alpha(\mathbf{k}) - \xi_\alpha(\mathbf{k}) \widehat{u}_\beta(\mathbf{k})) \varphi_{\mathbf{k}}, \quad \text{div } \mathbf{u} = \sum_{\mathbf{k} \in \mathbb{Z}^d} 2\pi i (\boldsymbol{\xi}(\mathbf{k}), \widehat{\mathbf{u}}(\mathbf{k}))_{\mathbb{C}^d} \varphi_{\mathbf{k}},$$

cf. [16, pp. 2–3] and [30]. Furthermore, the constant functions from \mathcal{U} are naturally identified with vectors from \mathbb{R}^d .

Alternatively, the subspaces arising in the Helmholtz decomposition (12) can be characterized by the orthogonal projections introduced below.

Definition 1. Let $\mathcal{G}^{\mathcal{U}}$, $\mathcal{G}^{\mathcal{E}}$, and $\mathcal{G}^{\mathcal{J}}$ denote operators $L^2_{\#}(\mathcal{Y}; \mathbb{R}^d) \rightarrow L^2_{\#}(\mathcal{Y}; \mathbb{R}^d)$ defined via

$$\mathcal{G}^{\bullet}[v](\mathbf{x}) = \sum_{\mathbf{k} \in \mathbb{Z}^d} \hat{\Gamma}^{\bullet}(\mathbf{k}) \hat{v}(\mathbf{k}) \varphi_{\mathbf{k}}(\mathbf{x}) \quad \text{for } \bullet \in \{\mathcal{U}, \mathcal{E}, \mathcal{J}\},$$

where the matrices of Fourier coefficients $\hat{\Gamma}^{\bullet}(\mathbf{k}) \in \mathbb{R}^{d \times d}$ read

$$\hat{\Gamma}^{\mathcal{U}}(\mathbf{k}) = \begin{cases} \mathbf{I} \\ \mathbf{0} \otimes \mathbf{0} \end{cases} \quad \hat{\Gamma}^{\mathcal{E}}(\mathbf{k}) = \begin{cases} \mathbf{0} \otimes \mathbf{0} \\ \frac{\boldsymbol{\xi}(\mathbf{k}) \otimes \boldsymbol{\xi}(\mathbf{k})}{\boldsymbol{\xi}(\mathbf{k}) \cdot \boldsymbol{\xi}(\mathbf{k})} \end{cases} \quad \hat{\Gamma}^{\mathcal{J}}(\mathbf{k}) = \begin{cases} \mathbf{0} \otimes \mathbf{0}, & \text{for } \mathbf{k} = \mathbf{0} \\ \mathbf{I} - \frac{\boldsymbol{\xi}(\mathbf{k}) \otimes \boldsymbol{\xi}(\mathbf{k})}{\boldsymbol{\xi}(\mathbf{k}) \cdot \boldsymbol{\xi}(\mathbf{k})} & \text{for } \mathbf{k} \in \mathbb{Z}^d \setminus \{\mathbf{0}\} \end{cases}.$$

Lemma 2. Operators $\mathcal{G}^{\mathcal{U}}$, $\mathcal{G}^{\mathcal{E}}$, and $\mathcal{G}^{\mathcal{J}}$ are mutually orthogonal projections with respect to the inner product on $L^2_{\#}(\mathcal{Y}; \mathbb{R}^d)$, on \mathcal{U} , \mathcal{E} , and \mathcal{J} .

Proof. In [22, Lemma 3.2], the authors show in detail that $\mathcal{G}^{\mathcal{E}}$ is an orthogonal projection onto \mathcal{E} . The remaining cases follow from the mutual orthogonality of $\hat{\Gamma}^{\bullet}(\mathbf{k}) : \mathbb{C}^d \rightarrow \mathbb{C}^d$ for all $\mathbf{k} \in \mathbb{Z}^d$ and with $\bullet \in \{\mathcal{U}, \mathcal{E}, \mathcal{J}\}$, cf. [41, section 12.1]. \square

3 Continuous homogenization problem and its discretization

3.1 Continuous formulation

Here and in the next sections, matrix field $\mathbf{A} : \mathcal{Y} \rightarrow \mathbb{R}_{\text{spd}}^{d \times d}$ is reserved for material coefficients which are required to be essentially bounded, symmetric, and uniformly elliptic:

$$\mathbf{A} \in L^{\infty}_{\#}(\mathcal{Y}; \mathbb{R}_{\text{spd}}^{d \times d}), \quad c_A \|\mathbf{v}\|_{\mathbb{R}^d}^2 \leq (\mathbf{A}(\mathbf{x})\mathbf{v}, \mathbf{v})_{\mathbb{R}^d} \leq C_A \|\mathbf{v}\|_{\mathbb{R}^d}^2, \quad (13)$$

almost everywhere in \mathcal{Y} and for all $\mathbf{v} \in \mathbb{R}^d$ with $0 < c_A \leq C_A < +\infty$. By $\rho_A = C_A/c_A$, the author denotes the condition number quantifying the contrast in coefficients \mathbf{A} . Using (6), the inverse coefficients satisfy

$$\mathbf{A}^{-1} \in L^{\infty}_{\#}(\mathcal{Y}; \mathbb{R}_{\text{spd}}^{d \times d}), \quad \frac{1}{C_A} \|\mathbf{v}\|_{\mathbb{R}^d}^2 \leq (\mathbf{A}^{-1}(\mathbf{x})\mathbf{v}, \mathbf{v})_{\mathbb{R}^d} \leq \frac{1}{c_A} \|\mathbf{v}\|_{\mathbb{R}^d}^2$$

a.e. in \mathcal{Y} for all $\mathbf{v} \in \mathbb{R}^d$.

Employing material coefficients, bilinear forms $a, a^{-1} : L^2_{\#}(\mathcal{Y}; \mathbb{R}^d) \times L^2_{\#}(\mathcal{Y}; \mathbb{R}^d) \rightarrow \mathbb{R}$ are defined as

$$a(\mathbf{u}, \mathbf{v}) := (\mathbf{A}\mathbf{u}, \mathbf{v})_{L^2_{\#}(\mathcal{Y}; \mathbb{R}^d)} \quad a^{-1}(\mathbf{u}, \mathbf{v}) := (\mathbf{A}^{-1}\mathbf{u}, \mathbf{v})_{L^2_{\#}(\mathcal{Y}; \mathbb{R}^d)}. \quad (14)$$

Next, the author defines homogenization problem (1a) in both primal and dual formulations.

Definition 3 (Homogenized matrices). Let material coefficients satisfy (13). Then the primal and the dual homogenized matrices $\mathbf{A}_H, \mathbf{B}_H \in \mathbb{R}^{d \times d}$ satisfy

$$(\mathbf{A}_H \mathbf{E}, \mathbf{E})_{\mathbb{R}^d} = \min_{\mathbf{e} \in \mathcal{E}} a(\mathbf{E} + \mathbf{e}, \mathbf{E} + \mathbf{e}) = a(\mathbf{E} + \mathbf{e}^{(\mathbf{E})}, \mathbf{E} + \mathbf{e}^{(\mathbf{E})}), \quad (15a)$$

$$(\mathbf{B}_H \mathbf{J}, \mathbf{J})_{\mathbb{R}^d} = \min_{\mathbf{j} \in \mathcal{J}} a^{-1}(\mathbf{J} + \mathbf{j}, \mathbf{J} + \mathbf{j}) = a^{-1}(\mathbf{J} + \mathbf{j}^{(\mathbf{J})}, \mathbf{J} + \mathbf{j}^{(\mathbf{J})}) \quad (15b)$$

for arbitrary quantities $\mathbf{E}, \mathbf{J} \in \mathbb{R}^d$ and minimizers $\mathbf{e}^{(\mathbf{E})}$ and $\mathbf{j}^{(\mathbf{J})}$.

3.2 Observations

Remark 4. The minimizers $\mathbf{e}^{(\mathbf{E})}$ and $\mathbf{j}^{(\mathbf{J})}$ — thanks to the Lax-Milgram theorem — exist, are unique for any $\mathbf{E}, \mathbf{J} \in \mathbb{R}^d$, and satisfy the optimality condition

$$a(\mathbf{e}^{(\mathbf{E})}, \mathbf{v}) = -a(\mathbf{E}, \mathbf{v}) \quad \forall \mathbf{v} \in \mathcal{E}, \quad a^{-1}(\mathbf{j}^{(\mathbf{J})}, \mathbf{v}) = -a^{-1}(\mathbf{J}, \mathbf{v}) \quad \forall \mathbf{v} \in \mathcal{J}.$$

Remark 5. Notice that the primal formulation (15a) coincides with problem (1a) introduced in section 1, because the subspace \mathcal{E} from (12b) admits an equivalent characterization $\mathcal{E} = \{\nabla f : f \in H_{\#, (0)}^1\}$, cf. [16, pp. 6–7].

Remark 6 (Properties of homogenized coefficients). The homogenized matrices $\mathbf{A}_H, \mathbf{B}_H$ from (15) are symmetric, positive definite, and thus invertible in accordance with the periodic homogenization theory, e.g. [15, 16, 17].

Remark 7 (Components of homogenized coefficients). The components of the homogenized matrix, defined in (15), can be evaluated according to

$$\mathbf{A}_{H, \alpha\beta} = a(\mathbf{U}^{(\alpha)} + \mathbf{e}^{(\alpha)}, \mathbf{U}^{(\beta)} + \mathbf{e}^{(\beta)}), \quad \mathbf{B}_{H, \alpha\beta} = a^{-1}(\mathbf{U}^{(\alpha)} + \mathbf{j}^{(\alpha)}, \mathbf{U}^{(\beta)} + \mathbf{j}^{(\beta)}),$$

where $\mathbf{U}^{(\alpha)} = (\delta_{\alpha\beta})_{\beta} \in \mathbb{R}^d$ and the fields $\mathbf{e}^{(\alpha)} \in \mathcal{E}$, $\mathbf{j}^{(\alpha)} \in \mathcal{J}$ are solutions of the following auxiliary problems

$$a(\mathbf{e}^{(\alpha)}, \mathbf{v})_{L_{\#}^2} = -a(\mathbf{U}^{(\alpha)}, \mathbf{v})_{L_{\#}^2} \quad \forall \mathbf{v} \in \mathcal{E}, \quad (16a)$$

$$a^{-1}(\mathbf{j}^{(\alpha)}, \mathbf{v})_{L_{\#}^2} = -a^{-1}(\mathbf{U}^{(\alpha)}, \mathbf{v})_{L_{\#}^2} \quad \forall \mathbf{v} \in \mathcal{J}. \quad (16b)$$

Remark 8 (Consequences of linearity and duality). The homogenized matrices are mutually inverse

$$\mathbf{A}_H = \mathbf{B}_H^{-1},$$

in compliance with standard duality arguments [54]. Moreover, the minimizers $\mathbf{e}^{(\mathbf{E})} \in \mathcal{E}$ and $\mathbf{j}^{(\mathbf{J})} \in \mathcal{J}$ of the homogenization problems (15) for $\mathbf{E}, \mathbf{J} \in \mathbb{R}^d$ can be obtained, due to a linear structure, from auxiliary minimizers defined in (16), i.e.

$$\mathbf{e}^{(\mathbf{E})} = \sum_{\alpha} E_{\alpha} \mathbf{e}^{(\alpha)}, \quad \mathbf{j}^{(\mathbf{J})} = \sum_{\alpha} J_{\alpha} \mathbf{j}^{(\alpha)}.$$

Moreover, the dual auxiliary field $\mathbf{j}^{(\beta)}$ from (16) can be expressed as a linear combination of primal ones $\mathbf{e}^{(\alpha)}$, so

$$\mathbf{U}^{(\beta)} + \mathbf{j}^{(\beta)} = \mathbf{A} \sum_{\alpha} E_{\alpha} \mathbf{e}^{(\alpha)} \quad \text{for } \mathbf{E} = \mathbf{A}_H^{-1} \mathbf{U}^{(\beta)} \in \mathbb{R}^d.$$

Remark 9 (Discrete problems). Remarks 4, 6, 7, and 8 introduced in this section for the continuous homogenization problem (15) are also applicable to the discrete relatives described in the following section 3.3. They have been studied in [9] for Galerkin approximation with numerical integration (19) and also hold true — especially Remarks 4, 6, and 7 — with the Galerkin approximation scheme (18).

3.3 Galerkin approximations

This section describes the discretization of the homogenization problem (15) utilizing the Galerkin method with an approximation space consisting of trigonometric polynomials

$$\mathcal{T}_N^d = \left\{ \sum_{\mathbf{k} \in \overset{\circ}{\mathbb{Z}}_N^d} \hat{\mathbf{v}}_N^{\mathbf{k}} \varphi_{\mathbf{k}} : \hat{\mathbf{v}}_N^{\mathbf{k}} = \overline{(\hat{\mathbf{v}}_N^{-\mathbf{k}})} \in \mathbb{C}^d \right\} \quad \text{for } \overset{\circ}{\mathbb{Z}}_N^d = \left\{ \mathbf{k} \in \mathbb{Z}^d : -\frac{N_\alpha}{2} < k_\alpha < \frac{N_\alpha}{2} \right\},$$

where the Fourier basis functions $\varphi_{\mathbf{k}}(\mathbf{x}) = \exp\left(2\pi i \sum_\alpha \frac{k_\alpha x_\alpha}{Y_\alpha}\right)$ were already defined in (8) when treating the Fourier series, and where vector $\mathbf{N} \in \mathbb{N}^d$ denotes their order and also the number of grid points on which they are uniquely defined; for an explanation, see Appendix A.

Unfortunately, the Fourier basis functions for Nyquist frequencies $\pm \frac{N_\alpha}{2}$ cause a nonconformity of approximation space, which is important when evaluating the guaranteed bounds on homogenized properties. These basis functions become complex valued; the conjugate symmetry of Fourier coefficients is lost for those frequencies. The problem has been identified in [31, section 2.4] regarding the divergence-free convergence criterion applied on dual fields (current, stress), cf. [9, Remark 43] for a detailed discussion. As a remedy, according to my previous work [9, section 4.2], these frequencies are omitted from the index set $\overset{\circ}{\mathbb{Z}}_N^d$; thus, only polynomials of odd degree (defined on odd grids), i.e.

$$\mathbf{N} \in \mathbb{N}^d \quad \text{such that } N_\alpha \text{ is odd for all } \alpha, \quad (17)$$

are considered in the approximation space.

Generally, the difficulties in a conforming discretization of the continuous homogenization problem (15) arise when approximating Helmholtz decomposition subspaces (11), especially in dual formulations for the space of divergence free fields; the approximation of curl-free space \mathcal{E} in the primal formulation can be resolved with a conforming approximation of the space of potentials. Luckily, Helmholtz decomposition (11) is transferred to trigonometric polynomials

$$\mathcal{T}_N^d = \mathcal{U} \oplus \mathcal{E}_N \oplus \mathcal{J}_N \quad \text{such that } \mathcal{E}_N \subset \mathcal{E} \text{ and } \mathcal{J}_N \subset \mathcal{J},$$

which can be performed by the orthogonal projections $\mathcal{G}^{\mathcal{U}}$, $\mathcal{G}^{\mathcal{E}}$, $\mathcal{G}^{\mathcal{J}}$ introduced in Definition 1 for the continuous problem. Using the truncation operator \mathcal{P}_N defined in (59), the discretization strategy is represented in Figure 1 as a commutative diagram. Moreover, these projections enable not only a proper discretization but also an effective numerical treatment of discrete problems.

$$\begin{array}{ccc} \mathcal{J} & \xrightarrow{\mathcal{P}_N} & \mathcal{J}_N \\ \mathcal{G}^{\mathcal{U}} \uparrow & & \mathcal{G}^{\mathcal{U}} \uparrow \\ L_{\text{per}}^2(\mathcal{Y}; \mathbb{R}^d) & \xrightarrow{\mathcal{P}_N} & \mathcal{T}_N^d \\ \mathcal{G}^{\mathcal{E}} \downarrow & & \mathcal{G}^{\mathcal{E}} \downarrow \\ \mathcal{E} & \xrightarrow{\mathcal{P}_N} & \mathcal{E}_N \end{array}$$

Figure 1: Discretization strategy

Then, the discrete homogenized problems are represented with two schemes, the Galerkin approximation (Ga) introduced in [22, Definition 5] and by its version with numerical integration (GaNi) introduced in [22, Definition 7] for an odd number of grid points (17) and in [9, Definition 29] for a general number of grid points.

Definition 10 (Galerkin approximation — Ga). *The primal and the dual homogenization matrices $\mathbf{A}_{\text{H},N}, \mathbf{B}_{\text{H},N} \in \mathbb{R}^{d \times d}$ of Ga satisfy*

$$(\mathbf{A}_{\text{H},N} \mathbf{E}, \mathbf{E})_{\mathbb{R}^d} = \inf_{\mathbf{e}_N \in \mathcal{E}_N} a(\mathbf{E} + \mathbf{e}_N, \mathbf{E} + \mathbf{e}_N) = a(\mathbf{E} + \mathbf{e}_N^{(\mathbf{E})}, \mathbf{E} + \mathbf{e}_N^{(\mathbf{E})}) \quad (18a)$$

$$(\mathbf{B}_{\text{H},N} \mathbf{J}, \mathbf{J})_{\mathbb{R}^d} = \inf_{\mathbf{j}_N \in \mathcal{J}_N} a^{-1}(\mathbf{J} + \mathbf{j}_N, \mathbf{J} + \mathbf{j}_N) = a^{-1}(\mathbf{J} + \mathbf{j}_N^{(\mathbf{J})}, \mathbf{J} + \mathbf{j}_N^{(\mathbf{J})}) \quad (18b)$$

for arbitrary quantities $\mathbf{E}, \mathbf{J} \in \mathbb{R}^d$.

Remark 11. *Notice that the primal formulation (18a) coincides with the problem (3a) introduced in section 1, because the subspace \mathcal{E}_N from Definition (48) admits an equivalent characterization $\mathcal{E}_N = \{\nabla f : f \in \mathcal{T}_N\}$ or alternatively $\mathcal{E}_N = \mathcal{E} \cap \mathcal{T}_N^d$ in accordance with Remark 50.*

Evaluation of the integrals in (15), described in section 4, is generally unfeasible in closed form. This weakness can be compensated for with the trapezoidal integration rule carried out by the interpolation operator $\mathcal{Q}_N : C_{\#}^0(\mathcal{Y}; \mathbb{R}^d) \rightarrow \mathcal{T}_N^d$ defined in (59). The bilinear forms (14) are then approximated to operators $\tilde{a}_N, \tilde{a}_N^{-1} : \mathcal{T}_N^d \times \mathcal{T}_N^d \rightarrow \mathbb{R}$ expressed as

$$\begin{aligned} \tilde{a}_N(\mathbf{u}_N, \mathbf{v}_N) &:= (\mathcal{Q}_N[\mathbf{A}\mathbf{u}_N], \mathbf{v}_N)_{L_{\#}^2(\mathcal{Y}; \mathbb{R}^d)}, \\ \tilde{a}_N^{-1}(\mathbf{u}_N, \mathbf{v}_N) &:= (\mathcal{Q}_N[\mathbf{A}^{-1}\mathbf{u}_N], \mathbf{v}_N)_{L_{\#}^2(\mathcal{Y}; \mathbb{R}^d)}. \end{aligned}$$

Noting that the objects related to this numerical integration are consistently denoted with the tilde symbol, e.g. $\tilde{a}_N, \tilde{\mathbf{A}}_{\text{H},N}$, or $\tilde{\mathbf{A}}_{\text{H},N}^{\text{GaNi}}$.

Definition 12 (Galerkin approximation with numerical integration — GaNi). *Let material coefficients (13) be additionally continuous $\mathbf{A} \in C_{\#}^0(\mathcal{Y}; \mathbb{R}_{\text{spd}}^{d \times d})$. Then, the primal and the dual homogenized coefficients $\tilde{\mathbf{A}}_{\text{H},N}^{\text{GaNi}}, \tilde{\mathbf{B}}_{\text{H},N}^{\text{GaNi}} \in \mathbb{R}^{d \times d}$ satisfy*

$$(\tilde{\mathbf{A}}_{\text{H},N}^{\text{GaNi}} \mathbf{E}, \mathbf{E})_{\mathbb{R}^d} = \inf_{\mathbf{e}_N \in \mathcal{E}_N} \tilde{a}_N(\mathbf{E} + \mathbf{e}_N, \mathbf{E} + \mathbf{e}_N) = \tilde{a}_N(\mathbf{E} + \tilde{\mathbf{e}}_N^{(\mathbf{E})}, \mathbf{E} + \tilde{\mathbf{e}}_N^{(\mathbf{E})}), \quad (19a)$$

$$(\tilde{\mathbf{B}}_{\text{H},N}^{\text{GaNi}} \mathbf{J}, \mathbf{J})_{\mathbb{R}^d} = \inf_{\mathbf{j}_N \in \mathcal{J}_N} \tilde{a}_N^{-1}(\mathbf{J} + \mathbf{j}_N, \mathbf{J} + \mathbf{j}_N) = \tilde{a}_N^{-1}(\mathbf{J} + \tilde{\mathbf{j}}_N^{(\mathbf{J})}, \mathbf{J} + \tilde{\mathbf{j}}_N^{(\mathbf{J})}), \quad (19b)$$

for arbitrary quantities $\mathbf{E}, \mathbf{J} \in \mathbb{R}^d$.

Remark 13 (Duality in GaNi). *Surprisingly, according to [9, Proposition 34], the duality from the continuous formulation discussed in Remark 8 is inherited in the GaNi for the odd grids (17), particularly*

$$(\tilde{\mathbf{B}}_{\text{H},N}^{\text{GaNi}})^{-1} = \tilde{\mathbf{A}}_{\text{H},N}^{\text{GaNi}}.$$

In [9, section 6], the minimizers of the GaNi scheme $\tilde{\mathbf{e}}_N^{(\mathbf{E})}, \tilde{\mathbf{j}}_N^{(\mathbf{J})}$ were used to a posteriori define the approximate homogenized coefficients

$$(\tilde{\mathbf{A}}_{\text{H},N} \mathbf{E}, \mathbf{E})_{\mathbb{R}^d} = a(\mathbf{E} + \tilde{\mathbf{e}}_N^{(\mathbf{E})}, \mathbf{E} + \tilde{\mathbf{e}}_N^{(\mathbf{E})}), \quad (20a)$$

$$(\tilde{\mathbf{B}}_{\text{H},N} \mathbf{J}, \mathbf{J})_{\mathbb{R}^d} = a^{-1}(\mathbf{J} + \tilde{\mathbf{j}}_N^{(\mathbf{J})}, \mathbf{J} + \tilde{\mathbf{j}}_N^{(\mathbf{J})}). \quad (20b)$$

holding for all $\mathbf{E}, \mathbf{J} \in \mathbb{R}^d$. In the next section, the author shows that these matrices are guaranteed bounds on homogenized coefficients.

3.4 Structure of guaranteed bounds on homogenized properties

In our previous work [9, section 6], the authors have shown the relation between homogenized coefficients of continuous formulation (15) and of the guaranteed bounds defined with the GaNi minimizers in (20), i.e.

$$\tilde{\mathbf{B}}_{\mathbf{H},\mathbf{N}}^{-1} \preceq \mathbf{B}_{\mathbf{H}}^{-1} = \mathbf{A}_{\mathbf{H}} \preceq \tilde{\mathbf{A}}_{\mathbf{H},\mathbf{N}}.$$

Here, this structure is extended for the homogenized coefficients defined with the Ga scheme (18).

Theorem 14 (Structure of guaranteed bounds). *The homogenized coefficients occurring in equations (15), (18), and (20) have the following structure*

$$\tilde{\mathbf{B}}_{\mathbf{H},\mathbf{N}}^{-1} \preceq \mathbf{B}_{\mathbf{H},\mathbf{N}}^{-1} \preceq \mathbf{B}_{\mathbf{H}}^{-1} = \mathbf{A}_{\mathbf{H}} \preceq \mathbf{A}_{\mathbf{H},\mathbf{N}} \preceq \tilde{\mathbf{A}}_{\mathbf{H},\mathbf{N}}. \quad (21)$$

Proof. First of all, the proof of inequality $\mathbf{A}_{\mathbf{H}} \preceq \mathbf{A}_{\mathbf{H},\mathbf{N}}$ is based on the conformity of approximate space $\mathcal{E}_{\mathbf{N}} \subset \mathcal{E}$, cf. Figure 11 and its proof in Lemma 49. Indeed, as the minimization space of the homogenization problem (15a) is reduced, the minimum has to remain or increase, i.e.

$$(\mathbf{A}_{\mathbf{H}}\mathbf{E}, \mathbf{E})_{\mathbb{R}^d} = \inf_{\mathbf{e} \in \mathcal{E}} a(\mathbf{E} + \mathbf{e}, \mathbf{E} + \mathbf{e}) \leq \inf_{\mathbf{e}_{\mathbf{N}} \in \mathcal{E}_{\mathbf{N}}} a(\mathbf{E} + \mathbf{e}_{\mathbf{N}}, \mathbf{E} + \mathbf{e}_{\mathbf{N}}) = (\mathbf{A}_{\mathbf{H},\mathbf{N}}\mathbf{E}, \mathbf{E})_{\mathbb{R}^d}.$$

Now, the following inequality $\mathbf{A}_{\mathbf{H},\mathbf{N}} \preceq \tilde{\mathbf{A}}_{\mathbf{H},\mathbf{N}}$ is proven by substituting the minimizer $\mathbf{e}_{\mathbf{N}}^{(\mathbf{E})}$ in the GA scheme (18a) with the approximate minimizers $\tilde{\mathbf{e}}_{\mathbf{N}}^{(\mathbf{E})}$ of the GaNi scheme (19a), i.e.

$$(\mathbf{A}_{\mathbf{H},\mathbf{N}}\mathbf{E}, \mathbf{E})_{\mathbb{R}^d} = \inf_{\mathbf{e}_{\mathbf{N}} \in \mathcal{E}_{\mathbf{N}}} a(\mathbf{E} + \mathbf{e}_{\mathbf{N}}, \mathbf{E} + \mathbf{e}_{\mathbf{N}}) \leq a(\mathbf{E} + \tilde{\mathbf{e}}_{\mathbf{N}}^{(\mathbf{E})}, \mathbf{E} + \tilde{\mathbf{e}}_{\mathbf{N}}^{(\mathbf{E})}) = (\tilde{\mathbf{A}}_{\mathbf{H},\mathbf{N}}\mathbf{E}, \mathbf{E})_{\mathbb{R}^d}.$$

Since the primal inequalities $\mathbf{A}_{\mathbf{H}} \preceq \mathbf{A}_{\mathbf{H},\mathbf{N}} \preceq \tilde{\mathbf{A}}_{\mathbf{H},\mathbf{N}}$ are in hand, the dual formulation reveals the upper bounds on the dual matrix

$$\mathbf{B}_{\mathbf{H}} \preceq \mathbf{B}_{\mathbf{H},\mathbf{N}} \preceq \tilde{\mathbf{B}}_{\mathbf{H},\mathbf{N}}.$$

The proof then arises from the inverse inequality (6) and from the duality of the continuous homogenization problem

$$\mathbf{B}_{\mathbf{H}}^{-1} = \mathbf{A}_{\mathbf{H}},$$

which follows by the standard duality arguments in [54, 55] or [9, Proposition 7 and Corollary 9]. \square

4 Numerical integration

The calculation of the guaranteed bounds on the homogenized coefficients (21) consists of the evaluation of bilinear forms (14) occurring in the formulation of the Ga scheme (18) or in the a posteriori estimate with the GaNi minimizers (20), i.e. integrals of the type

$$(\mathbf{A}\mathbf{u}_{\mathbf{N}}, \mathbf{v}_{\mathbf{N}})_{L^2_{\#}(\mathcal{Y}; \mathbb{R}^d)} \quad \text{for } \mathbf{A} \in L^{\infty}_{\#}(\mathcal{Y}; \mathbb{R}^{d \times d}) \text{ and } \mathbf{u}_{\mathbf{N}}, \mathbf{v}_{\mathbf{N}} \in \mathcal{T}_{\mathbf{N}}^d \quad (22)$$

for an odd grid assumption (17). Because the minimizers of both the Ga (18) and GaNi (19) schemes are from the space $\mathcal{T}_{\mathbf{N}}^d$ defined in (53a), this restriction is without loss of generality.

This integral evaluation based on double grid quadrature has already been analyzed in [9, section 6], which is summarized in section 4.2 for a matrix-inclusion composite (25). Then, in

section 4.3, the methodology is generalized to an effective evaluation of integral (22) for grid-based composites, which are defined via high-resolution images assuming piece-wise constant or piece-wise bilinear material coefficients.

Comparing the evaluation of the GaNi scheme (19) with the integral (22) occurring in the Ga scheme (18), both schemes lead to the same fully discrete structure, although the latter form is evaluated on a double grid, cf. Lemma 16 and 21, resulting in higher memory and computational requirements. In section 4.4, the reduction from a double to an original grid is provided using shifts of DFT (58); this reduces memory requirements while the computational demands for calculating minimizers remain similar.

Generally, the bounds can be evaluated in closed form only for material coefficients having the analytical expression of Fourier coefficients. However, this class is sufficiently large, so this weakness can be resolved with proper approximation of the material coefficients, which still leads to guaranteed bounds; for details, see section 4.5.

4.1 Notation

A multi-index notation is systematically employed in which $\mathcal{X}^{\mathbf{N}}$ represents $\mathcal{X}^{N_1 \times \dots \times N_d}$ for $\mathbf{N} \in \mathbb{N}^d$. Then the sets $\mathbb{R}^{d \times \mathbf{N}}$ and $[\mathbb{R}^{d \times \mathbf{N}}]^2$ or their complex counterparts represent the space of vectors and matrices denoted by bold serif font, e.g. $\mathbf{v} = (v_\alpha^{\mathbf{k}})_{\alpha \in \mathbb{Z}_N^d} \in \mathbb{R}^{d \times \mathbf{N}}$ and $\mathbf{M} = (M_{\alpha\beta}^{\mathbf{k}\mathbf{m}})_{\alpha,\beta \in \mathbb{Z}_N^d} \in [\mathbb{R}^{d \times \mathbf{N}}]^2$ with the index set

$$\mathbb{Z}_N^d = \left\{ \mathbf{k} \in \mathbb{Z}^d : -\frac{N_\alpha}{2} \leq k_\alpha < \frac{N_\alpha}{2} \right\}.$$

Sub-vectors and sub-matrices are designated by superscripts, e.g. $\mathbf{v}^{\mathbf{k}} = (v_\alpha^{\mathbf{k}})_\alpha \in \mathbb{R}^d$ or $\mathbf{M}^{\mathbf{k}\mathbf{m}} = (M_{\alpha\beta}^{\mathbf{k}\mathbf{m}})_{\alpha,\beta} \in \mathbb{R}^{d \times d}$. The scalar products on $\mathbb{R}^{d \times \mathbf{N}}$ and $\mathbb{C}^{d \times \mathbf{N}}$ are defined as

$$(\mathbf{u}, \mathbf{v})_{\mathbb{R}^{d \times \mathbf{N}}} = \frac{1}{|\mathbf{N}|} \sum_{\mathbf{k} \in \mathbb{Z}_N^d} (\mathbf{u}^{\mathbf{k}}, \mathbf{v}^{\mathbf{k}})_{\mathbb{R}^d}, \quad (\mathbf{u}, \mathbf{v})_{\mathbb{C}^{d \times \mathbf{N}}} = \sum_{\mathbf{k} \in \mathbb{Z}_N^d} (\mathbf{u}^{\mathbf{k}}, \mathbf{v}^{\mathbf{k}})_{\mathbb{C}^d},$$

where $|\mathbf{N}| = \prod_\alpha N_\alpha$ stands for the number of discretization points. Moreover, the matrix-vector or matrix-matrix multiplications follow from

$$(\mathbf{M}\mathbf{v})^{\mathbf{k}} = \sum_{\mathbf{m} \in \mathbb{Z}_N^d} \mathbf{M}^{\mathbf{k}\mathbf{m}} \mathbf{v}^{\mathbf{m}} \in \mathbb{R}^d \quad \text{or} \quad (\mathbf{M}\mathbf{L})^{\mathbf{k}\mathbf{m}} = \sum_{\mathbf{n} \in \mathbb{Z}_N^d} \mathbf{M}^{\mathbf{k}\mathbf{n}} \mathbf{L}^{\mathbf{n}\mathbf{m}} \in \mathbb{R}^{d \times d},$$

for $\mathbf{k}, \mathbf{m} \in \mathbb{Z}_N^d$ and $\mathbf{L} \in [\mathbb{R}^{d \times \mathbf{N}}]^2$. Matrix $\mathbf{A} \in [\mathbb{R}^{d \times \mathbf{N}}]^2$, the linear operator on $\mathbb{R}^{d \times \mathbf{N}}$, is symmetric positive definite if

$$(\mathbf{A}\mathbf{u}, \mathbf{v})_{\mathbb{R}^{d \times \mathbf{N}}} = (\mathbf{u}, \mathbf{A}\mathbf{v})_{\mathbb{R}^{d \times \mathbf{N}}} \quad \text{and} \quad (\mathbf{A}\mathbf{v}, \mathbf{v})_{\mathbb{R}^{d \times \mathbf{N}}} > 0$$

holds for all $\mathbf{u}, \mathbf{v} \in \mathbb{R}^{d \times \mathbf{N}}$ such that $\mathbf{v} \neq \mathbf{0}$.

4.2 Methodology

The evaluation of integrals (22) involves providing formulas leading to a fully discrete version. The evaluation of bilinear forms in the conventional FEM leads to sparse matrices, which is also the case for the GaNi scheme (19) thanks to the orthogonality of basis functions (9) and (60c). In accordance with my previous work [9], more complicated scenarios arise with the Ga scheme (18) leading to a fully populated matrix on the original grid but a sparse matrix on the double grid; see following Lemmas 15 and 16 with the proofs in [9, Lemmas 35 and 37].

Lemma 15. For odd grid assumption (17), the integral (22) equals

$$(\mathbf{A}\mathbf{u}_N, \mathbf{v}_N)_{L^2_{\#}(\mathcal{Y}; \mathbb{R}^d)} = (\hat{\mathbf{A}}_N^{\text{full}} \hat{\mathbf{u}}_N, \hat{\mathbf{v}}_N)_{\mathbb{C}^{d \times N}} = (\mathbf{A}_N^{\text{full}} \mathbf{u}_N, \mathbf{v}_N)_{\mathbb{R}^{d \times N}}$$

where vectors $\mathbf{u}_N, \mathbf{v}_N \in \mathbb{R}^{d \times N}$ and $\hat{\mathbf{u}}_N, \hat{\mathbf{v}}_N \in \mathbb{C}^{d \times N}$ are defined via

$$\mathbf{u}_N = \mathcal{I}_N[\mathbf{u}_N], \quad \mathbf{v}_N = \mathcal{I}_N[\mathbf{v}_N], \quad \hat{\mathbf{u}}_N = \mathbf{F}_N \mathbf{u}_N, \quad \hat{\mathbf{v}}_N = \mathbf{F}_N \mathbf{v}_N,$$

and matrices $\mathbf{A}_N^{\text{full}} \in [\mathbb{R}^{d \times N}]^2$ and $\hat{\mathbf{A}}_N^{\text{full}} \in [\mathbb{C}^{d \times N}]^2$ as

$$(\hat{\mathbf{A}}_N^{\text{full}})^{kl} = \frac{1}{|\mathcal{Y}|} \int_{\mathcal{Y}} \mathbf{A}(\mathbf{x}) \varphi_{\mathbf{k}}(\mathbf{x}) \varphi_{-\mathbf{l}}(\mathbf{x}) d\mathbf{x} \quad \text{for } \mathbf{k}, \mathbf{l} \in \mathbb{Z}_N^d, \quad \mathbf{A}_N^{\text{full}} = \mathbf{F}_N \hat{\mathbf{A}}_N^{\text{full}} \mathbf{F}_N^{-1}.$$

Lemma 16 (Integral evaluation on a double grid). For odd grid assumption (17), the integral (22) equals

$$(\mathbf{A}\mathbf{u}_N, \mathbf{v}_N)_{L^2_{\#}(\mathcal{Y}; \mathbb{R}^d)} = (\mathbf{A}_{2N-1}^{\text{Ga}} \mathbf{u}_N, \mathbf{v}_N)_{\mathbb{R}^{d \times (2N-1)}}$$

where $\mathbf{u}_N = \mathcal{I}_{2N-1}[\mathbf{u}_N]$, $\mathbf{v}_N = \mathcal{I}_{2N-1}[\mathbf{v}_N] \in \mathbb{R}^{d \times (2N-1)}$, and $\mathbf{A}_{2N-1}^{\text{Ga}} \in [\mathbb{R}^{d \times (2N-1)}]^2$ with components

$$(\mathbf{A}_{2N-1}^{\text{Ga}})^{kl} = \delta_{kl} \sum_{\mathbf{m} \in \mathbb{Z}_{2N-1}^d} \omega_{2N-1}^{k\mathbf{m}} \hat{\mathbf{A}}(\mathbf{m}) \in \mathbb{R}^{d \times d} \quad (23)$$

In section 4.4, an analogical Lemma 21 for grid sizing $2N$ instead of $(2N - 1)$ can be found with a proof holding for both. This extended lemma is used in order to reduce the fully discrete scalar product to the original grid sizing N using shifts of DFT (58).

Remark 17 (Material coefficients leading to guaranteed bounds). The closed-form evaluation of integral (22) leading to the fully discrete matrices (23) or (29) rests upon recognition of the Fourier series expansion for material coefficients \mathbf{A} . The space of functions having analytical expression of Fourier coefficients constitutes a linear space thanks to the linearity of the Lebesgue integral. Three suitable candidates, which are also used for the numerical examples in section 6, are introduced here.

Let $\mathbf{h} \in \mathbb{R}^d$ and $r \in \mathbb{R}$ be parameters such that $0 < M_{\alpha} \leq Y_{\alpha}$ and $r \leq \min_{\alpha} Y_{\alpha}$, then the periodic functions $\text{rect}_{\mathbf{h}}, \text{tri}_{\mathbf{h}}, \text{circ}_r \in L^{\infty}_{\#}(\mathcal{Y}; \mathbb{R})$ are defined on \mathcal{Y} as

$$\text{rect}_{\mathbf{h}}(\mathbf{x}) = \begin{cases} 1 & \text{if } |x_{\alpha}| < \frac{h_{\alpha}}{2} \text{ for all } \alpha \\ 0 & \text{otherwise} \end{cases}, \quad (24a)$$

$$\text{tri}_{\mathbf{h}}(\mathbf{x}) = \prod_{\alpha} \max\{1 - |\frac{x_{\alpha}}{h_{\alpha}}|, 0\}, \quad (24b)$$

$$\text{circ}_r(\mathbf{x}) = \begin{cases} 1 & \text{for } \|\mathbf{x}\|_2 < r \\ 0 & \text{otherwise} \end{cases}, \quad (24c)$$

and comply with the following Fourier coefficients

$$\begin{aligned} \widehat{\text{rect}}_{\mathbf{h}}(\mathbf{m}) &= \frac{1}{|\mathcal{Y}|} \prod_{\alpha} h_{\alpha} \text{sinc}\left(\frac{h_{\alpha} m_{\alpha}}{Y_{\alpha}}\right), \\ \widehat{\text{tri}}_{\mathbf{h}}(\mathbf{m}) &= \frac{1}{|\mathcal{Y}|} \prod_{\alpha} h_{\alpha} \text{sinc}^2\left(\frac{h_{\alpha} m_{\alpha}}{Y_{\alpha}}\right), \\ \widehat{\text{circ}}_r(\mathbf{m}) &= \frac{1}{|\mathcal{Y}|} \begin{cases} \pi r^2 & \text{for } \mathbf{m} = \mathbf{0} \\ r^2 \frac{B_1(2\pi r \|\xi(\mathbf{m})\|_2)}{r \|\xi(\mathbf{m})\|_2} & \text{otherwise} \end{cases}, \end{aligned}$$

where $\text{sinc}(x) = \begin{cases} 1 & \text{for } x = 0 \\ \frac{\sin(\pi x)}{\pi x} & \text{for } x \neq 0 \end{cases}$ and B_1 is the Bessel function of the first kind.

The evaluation of the matrix in (23) necessitates the determination of Fourier coefficients $[\hat{\mathbf{A}}_{\alpha\beta}(\mathbf{m})]^{\mathbf{m} \in \mathbb{Z}_{2N-1}^d}$. This has been elaborated in detail in [9, Lemma 38], repeated here as Lemma 18, for the inclusion-matrix composites, characterized by coefficients in the form

$$\mathbf{A}(\mathbf{x}) = \mathbf{A}_{(0)} + \sum_{i=1}^n f_{(i)}(\mathbf{x} - \mathbf{x}_{(i)}) \mathbf{A}_{(i)} \quad (25)$$

where $\mathbf{A}_{(0)} \in \mathbb{R}^{d \times d}$ represents the coefficients of the matrix phase, matrices $\mathbf{A}_{(i)} \in \mathbb{R}^{d \times d}$ with functions $f_{(i)} \in L_{\#}^{\infty}(\mathcal{Y})$ for $i = 0, \dots, n$ quantify the distribution of coefficients within inclusions, centered at $\mathbf{x}_{(i)}$, along with their topology.

Lemma 18. *The matrix (23) for material coefficients (25) is given by*

$$\mathbf{A}_{2N-1}^{kl} = \delta_{kl} \left[\mathbf{A}_{(0)} + \sum_{i=1}^n \mathbf{A}_{(i)} \left(\sum_{\mathbf{m} \in \mathbb{Z}_{2N-1}^d} \omega_{2N-1}^{k\mathbf{m}} \varphi_{-\mathbf{m}}(\mathbf{x}_{(i)}) \hat{f}_{(i)}(\mathbf{m}) \right) \right] \in \mathbb{R}^{d \times d}, \quad (26)$$

where $\hat{f}_{(i)}(\mathbf{m})$ for $i \in \{1, \dots, n\}$ and $\mathbf{m} \in \mathbb{Z}_N^d$ denote the Fourier coefficients (7) of inclusion topologies $f_{(i)}$.

4.3 Material coefficients defined on grids

As an alternative to the inclusion-matrix composite (25), the grid-based composite is expressed as a linear combination of basis functions ψ concentrated on grid points $\mathbf{x}_{\mathbf{P}}^{\mathbf{m}}$ for $\mathbf{m} \in \mathbb{Z}_{\mathbf{P}}^d$ and $\mathbf{P} \in \mathbb{N}^d$, i.e.

$$\mathbf{A}(\mathbf{x}) = \sum_{\mathbf{m} \in \mathbb{Z}_{\mathbf{P}}^d} \psi(\mathbf{x} - \mathbf{x}_{\mathbf{P}}^{\mathbf{m}}) \mathbf{A}_{\mathbf{P}}^{\mathbf{m}} \quad \text{for } \mathbf{P} \in \mathbb{N}^d, \mathbf{x} \in \mathcal{Y}, \text{ and } \mathbf{A}_{\mathbf{P}} \in \mathbb{R}^{d \times d \times \mathbf{P}}. \quad (27)$$

The material resolution is systematically expressed by the symbol \mathbf{P} , which corresponds to the number of grid points and is generally different from the approximation order $N \in \mathbb{N}^d$ of trigonometric polynomials \mathcal{T}_N^d .

Remark 19. *The material coefficients (27) are represented with a pixel- or voxel-based image with a resolution $\mathbf{P} \in \mathbb{N}^d$. If the basis function ψ is taken as (24a) or (24b), the coefficients are piece-wise constant or bilinear, respectively.*

Lemma 20 (Grid-based composites). *The matrix (23) for material coefficients (27) is given by*

$$(\mathbf{A}_{2N-1}^{\text{Ga}})_{\alpha\beta}^{kl} = \delta_{kl} |\mathbf{P}| \sum_{\mathbf{m} \in \mathbb{Z}_{2N-1}^d} \omega_{2N-1}^{k\mathbf{m}} \hat{\psi}(\mathbf{m}) \left(\sum_{\mathbf{n} \in \mathbb{Z}_{\mathbf{P}}^d} \frac{\omega_{\mathbf{P}}^{-mn}}{|\mathbf{P}|} \mathbf{A}_{\mathbf{P},\alpha\beta}^{\mathbf{n}} \right) \quad (28)$$

where $\hat{\psi}(\mathbf{n})$ for $\mathbf{n} \in \mathbb{Z}_N^d$ are the Fourier coefficients of ψ .

Proof. Using an affine substitution, the following formula for $\mathbf{m}, \mathbf{n} \in \mathbb{Z}^d$ is deduced

$$\frac{1}{|\mathcal{Y}|} \int_{\mathcal{Y}} \psi(\mathbf{x} - \mathbf{x}_{\mathbf{P}}^{\mathbf{n}}) \varphi_{-\mathbf{m}}(\mathbf{x}) \, d\mathbf{x} = \frac{1}{|\mathcal{Y}|} \int_{\mathcal{Y}} \psi(\mathbf{x}) \varphi_{-\mathbf{m}}(\mathbf{x} + \mathbf{x}_{\mathbf{P}}^{\mathbf{n}}) \, d\mathbf{x} = \hat{\psi}(\mathbf{m}) \omega_{\mathbf{P}}^{-mn}.$$

This, (23), and (27) enable calculation

$$\begin{aligned}
(\mathbf{A}_{2N-1}^{\text{Ga}})_{\alpha\beta}^{kl} &= \delta_{kl} \sum_{\mathbf{m} \in \mathbb{Z}_{2N-1}^d} \omega_{2N-1}^{k\mathbf{m}} \frac{1}{|\mathcal{Y}|} \int_{\mathcal{Y}} A_{P,\alpha\beta} \varphi_{-m}(\mathbf{x}) \, d\mathbf{x} \\
&= \delta_{kl} \sum_{\mathbf{m} \in \mathbb{Z}_{2N-1}^d} \omega_{2N-1}^{k\mathbf{m}} \sum_{\mathbf{n} \in \mathbb{Z}_P^d} A_{P,\alpha\beta}^{\mathbf{n}} \frac{1}{|\mathcal{Y}|} \int_{\mathcal{Y}} \psi(\mathbf{x} - \mathbf{x}_P^{\mathbf{n}}) \varphi_{-m}(\mathbf{x}) \, d\mathbf{x} \\
&= \delta_{kl} \sum_{\mathbf{m} \in \mathbb{Z}_{2N-1}^d} \omega_{2N-1}^{k\mathbf{m}} \sum_{\mathbf{n} \in \mathbb{Z}_P^d} A_{P,\alpha\beta}^{\mathbf{n}} \omega_P^{-m\mathbf{n}} \hat{\psi}(\mathbf{m}).
\end{aligned}$$

□

4.4 Reduction from a double to the original grid

In Lemma 16, the integral (22) occurring in the Ga scheme (18) has been evaluated on a grid of size $2N - 1$. Here, it is reformulated in auxiliary Lemma 21 to size $2N$ and then, with the help of DFT shifts, reduced in Lemma 22 to size N occurring also in the GaNi scheme, cf. Lemma 27. This procedure reduces memory requirements.

Lemma 21 (Integral evaluation on a double grid). *For an odd grid assumption (17), the integral (22) equals*

$$(\mathbf{A}\mathbf{u}_N, \mathbf{v}_N)_{L^2_{\#}(\mathcal{Y}; \mathbb{R}^d)} = (\mathbf{A}_{2N}^{\text{Ga}} \mathbf{u}_N, \mathbf{v}_N)_{\mathbb{R}^{d \times 2N}}$$

where $\mathbf{u}_N = \mathcal{I}_{2N}[\mathbf{u}_N]$, $\mathbf{v}_N = \mathcal{I}_{2N}[\mathbf{v}_N] \in \mathbb{R}^{d \times 2N}$, and $\mathbf{A}_{2N}^{\text{Ga}} \in [\mathbb{R}^{d \times 2N}]^2$ with components

$$(\mathbf{A}_{2N}^{\text{Ga}})^{kl} = \delta_{kl} \sum_{\mathbf{m} \in \mathbb{Z}_{2N-1}^d} \omega_{2N}^{k\mathbf{m}} \hat{\mathbf{A}}(\mathbf{m}) \in \mathbb{R}^{d \times d}. \quad (29)$$

Proof. Because the product of two trigonometric polynomials $\mathbf{u}_N \mathbf{v}_N = (u_{N,\alpha} v_{N,\alpha})_{\alpha} \in \mathcal{T}_{2N-1}^d$ has a bounded order by $2N - 1$, it can be expressed on both grids $2N - 1$ and $2N$ as

$$\begin{aligned}
u_{N,\beta} v_{N,\alpha} &= \sum_{\mathbf{n} \in \mathbb{Z}_{2N-1}^d} u_{N,\beta} \widehat{v_{N,\alpha}}(\mathbf{n}) \varphi_{\mathbf{n}} = \sum_{\mathbf{k} \in \mathbb{Z}_{2N-1}^d} u_{N,\beta}(\mathbf{x}_{2N-1}^{\mathbf{k}}) v_{N,\alpha}(\mathbf{x}_{2N-1}^{\mathbf{k}}) \varphi_{2N-1,\mathbf{k}} \\
&= \sum_{\mathbf{n} \in \mathbb{Z}_{2N}^d} u_{N,\beta} \widehat{v_{N,\alpha}}(\mathbf{n}) \varphi_{\mathbf{n}} = \sum_{\mathbf{k} \in \mathbb{Z}_{2N}^d} u_{N,\beta}(\mathbf{x}_{2N}^{\mathbf{k}}) v_{N,\alpha}(\mathbf{x}_{2N}^{\mathbf{k}}) \varphi_{2N,\mathbf{k}},
\end{aligned}$$

where $u_{N,\beta} \widehat{v_{N,\alpha}}(\mathbf{k}) = 0$ for $\mathbf{k} \in \mathbb{Z}_{2N}^d \setminus \mathbb{Z}_{2N-1}^d$.

Substitution into (22) and direct calculation reveals

$$\begin{aligned}
(\mathbf{A}\mathbf{u}_N, \mathbf{v}_N)_{L^2_{\#}} &= \sum_{\alpha,\beta} \sum_{\mathbf{n} \in \mathbb{Z}_{2N-1}^d} \hat{A}_{\alpha\beta}(-\mathbf{n}) u_{N,\alpha} \widehat{v_{N,\beta}}(\mathbf{n}) \\
&= \sum_{\alpha,\beta} \sum_{\mathbf{n} \in \mathbb{Z}_{2N-1}^d} \hat{A}_{\alpha\beta}(-\mathbf{n}) \sum_{\mathbf{k} \in \mathbb{Z}_{2N}^d} \frac{\omega_{2N}^{-\mathbf{n}\mathbf{k}}}{|2N|} u_{N,\alpha}(\mathbf{x}_{2N}^{\mathbf{k}}) v_{N,\beta}(\mathbf{x}_{2N}^{\mathbf{k}}).
\end{aligned}$$

The statement of the lemma follows by substituting \mathbf{n} with $-\mathbf{m}$. □

Lemma 22 (Reduction to the original grid). Let $\mathbb{S}^d = \prod_{\alpha} \{0, 1\}$ and $\mathbf{A}_{2N}^{\text{Ga}}$ be a matrix obtained from integral (22) in the previous Lemma 21. Then the fully discrete matrices in Lemma 15 can be reformulated to

$$\mathbf{A}^{\text{full}} = 2^{-d} \sum_{s \in \mathbb{S}^d} \mathbf{F}_N^{-1} \mathbf{S}_N^*(s) \mathbf{F}_N \mathbf{A}_N^{\text{Ga}}(s) \mathbf{F}_N^{-1} \mathbf{S}_N(s) \mathbf{F}_N, \quad (30a)$$

$$\hat{\mathbf{A}}^{\text{full}} = 2^{-d} \sum_{s \in \mathbb{S}^d} \mathbf{S}_N^*(s) \mathbf{F}_N^{-1} \mathbf{A}_N^{\text{Ga}}(s) \mathbf{F}_N \mathbf{S}_N(s), \quad (30b)$$

where the matrices $\mathbf{S}_N(s), \mathbf{A}_N^{\text{Ga}}(s) \in [\mathbb{C}^{d \times N}]^2$ are defined for $s \in \mathbb{S}^d$ as

$$\mathbf{S}_N(s) = (\delta_{\alpha\beta} \delta_{mn} \omega_{2N}^{-sm})_{\alpha,\beta}^{m,n \in \mathbb{Z}_N^d}, \quad \mathbf{A}_N^{\text{Ga}}(s) = (\delta_{kr} \mathbf{A}_{2N,\alpha\beta}^{\text{Ga},(2r-s)(2r-s)})_{\alpha,\beta}^{k,r \in \mathbb{Z}_N^d}.$$

Here, the matrices $\mathbf{A}_N(s)$ stand for the submatrices of $\mathbf{A}_{2N}^{\text{Ga}}$ and correspond to the shift matrices $\mathbf{S}_N(s)$.

Proof. According to Lemma 15 and 21, integral (22) can be expressed in three ways

$$(\mathbf{A} \mathbf{u}_N, \mathbf{v}_N)_{L^2_{\#}} = (\mathbf{A}_N^{\text{full}} \mathbf{u}_N, \mathbf{v}_N)_{\mathbb{R}^{d \times N}} = (\hat{\mathbf{A}}_N^{\text{full}} \hat{\mathbf{u}}_N, \hat{\mathbf{v}}_N)_{\mathbb{C}^{d \times N}} = (\mathbf{A}_{2N}^{\text{Ga}} \bar{\mathbf{u}}_N, \bar{\mathbf{v}}_N)_{\mathbb{R}^{d \times 2N}} \quad (31)$$

where

$$\mathbf{u}_N = \mathcal{I}_N^{-1}[\mathbf{u}_N] = \mathcal{I}_N^{-1}[\mathbf{F}_N^{-1} \hat{\mathbf{u}}_N] = \mathcal{I}_{2N}^{-1}[\hat{\mathbf{u}}_N], \quad \mathbf{v}_N = \mathcal{I}_N^{-1}[\mathbf{v}_N] = \mathcal{I}_N^{-1}[\mathbf{F}_N^{-1} \hat{\mathbf{v}}_N] = \mathcal{I}_{2N}^{-1}[\hat{\mathbf{v}}_N].$$

Now, the matrix $\mathbf{A}_{2N}^{\text{Ga}}$ will be decomposed to meet (30). In order to reduce the double grid sizing $2N$ to original grid sizing N , index $\mathbf{k} \in \mathbb{Z}_{2N}^d$ is uniquely split into

$$\mathbf{k} = 2\mathbf{r} - \mathbf{s} \quad \text{with } \mathbf{r} \in \mathbb{Z}_N^d \text{ and } \mathbf{s} \in \mathbb{S}. \quad (32)$$

Using the connection of the two representations of trigonometric polynomials via DFT stated in (57), it holds for $\mathbf{k} \in \mathbb{Z}_{2N}^d$ according to (32) that

$$\begin{aligned} \bar{\mathbf{u}}_N^{\mathbf{k}} &= \mathbf{u}_N(\mathbf{x}_{2N}^{\mathbf{k}}) = \sum_{\mathbf{m} \in \mathbb{Z}_N^d} \omega_{2N}^{\mathbf{k}\mathbf{m}} \hat{\mathbf{u}}_N(\mathbf{m}) \\ &= \bar{\mathbf{u}}_N^{2\mathbf{r}-\mathbf{s}} = \sum_{\mathbf{m} \in \mathbb{Z}_N^d} \omega_N^{\mathbf{r}\mathbf{m}} \omega_{2N}^{-\mathbf{s}\mathbf{m}} \hat{\mathbf{u}}_N(\mathbf{m}) = [\mathbf{F}_N^{-1} \mathbf{S}_N(s) \hat{\mathbf{u}}_N]^{\mathbf{r}}, \end{aligned}$$

where summation occurs only over \mathbb{Z}_N^d instead of \mathbb{Z}_{2N}^d since the trigonometric polynomial \mathbf{u}_N belongs to \mathcal{T}_N^d . Using the simplification $\mathbf{A}_{2N}^{\text{Ga},\mathbf{k}} := \mathbf{A}_{2N}^{\text{Ga},\mathbf{k}\mathbf{k}} \in \mathbb{R}^{d \times d}$ for $\mathbf{k} \in \mathbb{Z}_{2N}^d$, the bilinear form (31) can be reformulated into

$$\begin{aligned} (\mathbf{A}_{2N}^{\text{Ga}} \bar{\mathbf{u}}_N, \bar{\mathbf{v}}_N)_{\mathbb{R}^{d \times 2N}} &= \frac{1}{|2N|} \sum_{\mathbf{k} \in \mathbb{Z}_{2N}^d} (\mathbf{A}_{2N}^{\text{Ga},\mathbf{k}} \bar{\mathbf{u}}_N^{\mathbf{k}}, \bar{\mathbf{v}}_N^{\mathbf{k}})_{\mathbb{R}^d} \\ &= \frac{1}{|2N|} \sum_{\alpha,\beta} \sum_{s \in \mathbb{S}^d} \sum_{\mathbf{r} \in \mathbb{Z}_N^d} \mathbf{A}_{2N,\alpha\beta}^{\text{Ga},2\mathbf{r}-\mathbf{s}} \bar{\mathbf{u}}_{N,\beta}^{2\mathbf{r}-\mathbf{s}} \bar{\mathbf{v}}_{N,\alpha}^{2\mathbf{r}-\mathbf{s}} \\ &= \frac{1}{2^d |N|} \sum_{\alpha,\beta} \sum_{s \in \mathbb{S}^d} \sum_{\mathbf{r}, \mathbf{m}, \mathbf{n} \in \mathbb{Z}_N^d} \mathbf{A}_{2N,\alpha\beta}^{\text{Ga},2\mathbf{r}-\mathbf{s}} (\omega_N^{\mathbf{r}\mathbf{m}} \omega_{2N}^{-\mathbf{s}\mathbf{m}} \hat{\mathbf{u}}_{N,\beta}^{\mathbf{m}}) (\omega_N^{\mathbf{r}\mathbf{n}} \omega_{2N}^{-\mathbf{s}\mathbf{n}} \hat{\mathbf{v}}_{N,\alpha}^{\mathbf{n}}). \end{aligned}$$

In the latter brackets, the sign of index \mathbf{n} can be changed thanks to the symmetry of \mathbb{Z}_N^d for odd grids (17), i.e.

$$\mathbf{n} \in \mathbb{Z}_N^d \implies -\mathbf{n} \in \mathbb{Z}_N^d,$$

which allow for expressing summations as a scalar product on $\mathbb{C}^{d \times N}$, so

$$\begin{aligned} (\mathbf{A}_{2N}^{\text{Ga}} \bar{\mathbf{u}}_N, \bar{\mathbf{v}}_N)_{\mathbb{R}^{d \times 2N}} &= \frac{1}{2^d |N|} \sum_{\alpha, \beta} \sum_{\mathbf{s} \in \mathbb{S}^d} \sum_{\mathbf{r}, \mathbf{m}, \mathbf{n} \in \mathbb{Z}_N^d} A_{2N, \alpha\beta}^{\text{Ga}, 2r-s} (\omega_N^{r\mathbf{m}} \omega_{2N}^{-s\mathbf{m}} \hat{\mathbf{u}}_{N, \beta}^{\mathbf{m}}) (\omega_N^{-r\mathbf{n}} \omega_{2N}^{s\mathbf{n}} \hat{\mathbf{v}}_{N, \alpha}^{-\mathbf{n}}) \\ &= \frac{1}{2^d} \sum_{\alpha, \beta} \sum_{\mathbf{s} \in \mathbb{S}^d} \sum_{\mathbf{r}, \mathbf{m}, \mathbf{n} \in \mathbb{Z}_N^d} \frac{\overline{\omega_{2N}^{-s\mathbf{n}} \omega_N^{-r\mathbf{n}}}}{|N|} A_{2N, \alpha\beta}^{\text{Ga}, 2r-s} (\omega_N^{r\mathbf{m}} \omega_{2N}^{-s\mathbf{m}} \hat{\mathbf{u}}_{N, \beta}^{\mathbf{m}}) (\overline{\hat{\mathbf{v}}_{N, \alpha}^{-\mathbf{n}}}) \\ &= \frac{1}{2^d} \sum_{\mathbf{s} \in \mathbb{S}^d} (\mathbf{S}_N(\mathbf{s}) \mathbf{F}_N \mathbf{A}_N^{\text{Ga}}(\mathbf{s}) \mathbf{F}_N \mathbf{S}_N(\mathbf{s}) \hat{\mathbf{u}}_N, \hat{\mathbf{v}}_N)_{\mathbb{C}^{d \times N}} \end{aligned}$$

where the conjugate symmetry of $\hat{\mathbf{v}}_N$ and $\omega_{2N}^{s\mathbf{n}}$ has been used. Using Parseval's identity (10) in a discrete setting, it is reformulated as a scalar product on $\mathbb{R}^{d \times N}$

$$(\mathbf{A}_{2N}^{\text{Ga}} \bar{\mathbf{u}}_N, \bar{\mathbf{v}}_N)_{\mathbb{R}^{d \times 2N}} = \frac{1}{2^d} \sum_{\mathbf{s} \in \mathbb{S}^d} (\mathbf{F}_N^{-1} \mathbf{S}_N(\mathbf{s}) \mathbf{F}_N \mathbf{A}_N^{\text{Ga}}(\mathbf{s}) \mathbf{F}_N \mathbf{S}_N(\mathbf{s}) \mathbf{F}_N \mathbf{u}_N, \mathbf{v}_N)_{\mathbb{R}^{d \times N}}.$$

□

Remark 23. The previous lemma shows that the integral (22) can be evaluated on a grid of size N using the matrix $\mathbf{A}_{2N}^{\text{Ga}}$, see (29) in Lemma 21. However, the inclusion-matrix composite (25) and the grid-based composite (27) in Lemmas 18 and 20 resp. are evaluated only on a grid sizing $2N - 1$. Nevertheless, the proof for the grid of size N remains identical; therefore, only the formulas are stated here for both (25) and (27):

$$\begin{aligned} \mathbf{A}_{2N}^{kl} &= \delta_{kl} \left[\mathbf{A}_{(0)} + \sum_{i=1}^n \mathbf{A}_{(i)} \left(\sum_{\mathbf{m} \in \mathbb{Z}_{2N-1}^d} \omega_{2N}^{k\mathbf{m}} \varphi_{-\mathbf{m}}(\mathbf{x}_{(i)}) \hat{f}_{(i)}(\mathbf{m}) \right) \right] \in \mathbb{R}^{d \times d}, \\ (\mathbf{A}_{2N}^{\text{Ga}})_{\alpha\beta}^{kl} &= \delta_{kl} |2N| \sum_{\mathbf{m} \in \mathbb{Z}_{2N-1}^d} \omega_{2N}^{k\mathbf{m}} \hat{\psi}(\mathbf{m}) \left(\sum_{\mathbf{n} \in \mathbb{Z}_P^d} \frac{\omega_P^{-m\mathbf{n}}}{|P|} A_{P, \alpha\beta}^n \right). \end{aligned}$$

4.5 Approximation of guaranteed bounds

Throughout section 4, the author presents the methodology for evaluating guaranteed bounds on homogenized properties relying on determination of the matrix (23) or (29). For closed-form evaluation, an analytical expression of Fourier coefficients $\hat{A}_{\alpha\beta}(\mathbf{m})$ for $\mathbf{m} \in \mathbb{Z}_{2N-1}^d$ is required, cf. Remark 17.

For general material coefficients, an approximate calculation of the integral (22) can violate the structure of guaranteed bounds (21); this can be resolved by appropriate adjustment of the material coefficients presented in the following Lemma 24 with a particular example in Remark 25. This approach is inspired by [45, 46], which incorporated outer approximation of inclusion topology in the FEM framework.

Lemma 24 (Upper-upper and lower-lower guaranteed bounds). *Let $\bar{\mathbf{A}}, \underline{\mathbf{A}} \in L_{\#}^{\infty}(\mathcal{Y}; \mathbb{R}^{d \times d})$ be upper and lower approximations of material coefficients (13) satisfying*

$$\underline{\mathbf{A}}(\mathbf{x}) \preceq \mathbf{A}(\mathbf{x}) \preceq \bar{\mathbf{A}}(\mathbf{x}) \quad \text{for almost all } \mathbf{x} \in \mathcal{Y}, \quad (33)$$

and let $\bar{a}, \underline{a}^{-1} : L_{\#}^2(\mathcal{Y}; \mathbb{R}^d) \times L_{\#}^2(\mathcal{Y}; \mathbb{R}^d) \rightarrow \mathbb{R}$ be corresponding bilinear forms

$$\bar{a}(\mathbf{u}, \mathbf{v}) := (\bar{\mathbf{A}}\mathbf{u}, \mathbf{v})_{L_{\#}^2(\mathcal{Y}; \mathbb{R}^d)}, \quad \underline{a}^{-1}(\mathbf{u}, \mathbf{v}) := (\underline{\mathbf{A}}^{-1}\mathbf{u}, \mathbf{v})_{L_{\#}^2(\mathcal{Y}; \mathbb{R}^d)}.$$

Then matrices $\bar{\mathbf{A}}_{\mathbf{H}}, \underline{\mathbf{A}}_{\mathbf{H}}, \bar{\mathbf{A}}_{\mathbf{H},\mathbf{N}}, \underline{\mathbf{A}}_{\mathbf{H},\mathbf{N}} \in \mathbb{R}^{d \times d}$ defined for arbitrary quantities $\mathbf{E}, \mathbf{J} \in \mathbb{R}^d$

$$\begin{aligned} (\bar{\mathbf{A}}_{\mathbf{H}} \mathbf{E}, \mathbf{E})_{\mathbb{R}^d} &= \inf_{\mathbf{e} \in \mathcal{E}} \bar{a}(\mathbf{E} + \mathbf{e}, \mathbf{E} + \mathbf{e}), & (\bar{\mathbf{B}}_{\mathbf{H}} \mathbf{J}, \mathbf{J})_{\mathbb{R}^d} &= \inf_{\mathbf{j} \in \mathcal{J}} \underline{a}^{-1}(\mathbf{J} + \mathbf{j}, \mathbf{J} + \mathbf{j}), \\ (\bar{\mathbf{A}}_{\mathbf{H},\mathbf{N}} \mathbf{E}, \mathbf{E})_{\mathbb{R}^d} &= \inf_{\mathbf{e} \in \mathcal{E}_{\mathbf{N}}} \bar{a}(\mathbf{E} + \mathbf{e}, \mathbf{E} + \mathbf{e}), & (\bar{\mathbf{B}}_{\mathbf{H},\mathbf{N}} \mathbf{J}, \mathbf{J})_{\mathbb{R}^d} &= \inf_{\mathbf{j} \in \mathcal{J}_{\mathbf{N}}} \underline{a}^{-1}(\mathbf{J} + \mathbf{j}, \mathbf{J} + \mathbf{j}), \\ (\tilde{\mathbf{A}}_{\mathbf{H},\mathbf{N}} \mathbf{E}, \mathbf{E})_{\mathbb{R}^d} &= \bar{a}(\mathbf{E} + \tilde{\mathbf{e}}_{\mathbf{N}}^{(\mathbf{E})}, \mathbf{E} + \tilde{\mathbf{e}}_{\mathbf{N}}^{(\mathbf{E})}), & (\tilde{\mathbf{B}}_{\mathbf{H},\mathbf{N}} \mathbf{J}, \mathbf{J})_{\mathbb{R}^d} &= \underline{a}^{-1}(\mathbf{J} + \tilde{\mathbf{j}}_{\mathbf{N}}^{(\mathbf{J})}, \mathbf{J} + \tilde{\mathbf{j}}_{\mathbf{N}}^{(\mathbf{J})}) \end{aligned}$$

with minimizers $\tilde{\mathbf{e}}_{\mathbf{N}}^{(\mathbf{E})}, \tilde{\mathbf{j}}_{\mathbf{N}}^{(\mathbf{J})}$ of the GaNi scheme (19) comply with the following structure of guaranteed bounds, i.e.

$$\tilde{\mathbf{B}}_{\mathbf{H},\mathbf{N}}^{-1} \preceq \bar{\mathbf{B}}_{\mathbf{H},\mathbf{N}}^{-1} \preceq \begin{array}{c} \bar{\mathbf{B}}_{\mathbf{H}}^{-1} \\ \mathbb{R} \\ \mathbf{B}_{\mathbf{H},\mathbf{N}}^{-1} \end{array} \preceq \mathbf{B}_{\mathbf{H}}^{-1} = \mathbf{A}_{\mathbf{H}} \preceq \begin{array}{c} \bar{\mathbf{A}}_{\mathbf{H}} \\ \mathbb{R} \\ \mathbf{A}_{\mathbf{H},\mathbf{N}} \end{array} \preceq \bar{\mathbf{A}}_{\mathbf{H},\mathbf{N}} \preceq \tilde{\mathbf{A}}_{\mathbf{H},\mathbf{N}}.$$

Proof. The inner inequality $\mathbf{B}_{\mathbf{H},\mathbf{N}}^{-1} \preceq \mathbf{B}_{\mathbf{H}}^{-1} = \mathbf{A}_{\mathbf{H}} \preceq \mathbf{A}_{\mathbf{H},\mathbf{N}}$ has already been proven in Theorem 14. The rest easily arises from an assumed inequality (33) and the monotonicity of Lebesgue integration, i.e.

$$u, v \in L^1_{\#}(\mathcal{Y}), \quad u(\mathbf{x}) \leq v(\mathbf{x}) \text{ for almost all } \mathbf{x} \in \mathcal{Y} \quad \implies \quad \int_{\mathcal{Y}} u(\mathbf{x}) \, d\mathbf{x} \leq \int_{\mathcal{Y}} v(\mathbf{x}) \, d\mathbf{x}.$$

□

Remark 25 (Choice of $\bar{\mathbf{A}}$ and $\underline{\mathbf{A}}$). To comply with requirement (33) in the previous lemma, a possible choice of material coefficients consists of local approximations with piece-wise constant functions in a grid-based composite (27). This material is then characterized with a pixel- or voxel-based image defined via the following formula

$$\bar{\mathbf{A}} = \sum_{\mathbf{k} \in \mathbb{Z}_{\mathbf{P}}^d} \text{rect}_{\mathbf{h}}(\mathbf{x} - \mathbf{x}_{\mathbf{P}}^{\mathbf{k}}) \mathbf{A}_{\mathbf{P}}^{\mathbf{k}} \quad \text{with } \mathbf{A}_{\mathbf{P}}^{\mathbf{k}} = \|\mathbf{A}(\cdot - \mathbf{x}_{\mathbf{P}}^{\mathbf{k}})\|_{L^{\infty}_{\#}(\Omega_{\mathbf{h}}; \mathbb{R}^{d \times d})} \cdot \mathbf{I},$$

where vector $\mathbf{P} \in \mathbb{N}^d$ denotes an image resolution and where region $\Omega_{\mathbf{h}} = \Pi_{\alpha}(-\frac{h_{\alpha}}{2}, \frac{h_{\alpha}}{2})$ for $h_{\alpha} = \frac{Y_{\alpha}}{P_{\alpha}}$ represents a pixel or voxel placed at the origin with characteristic function $\text{rect}_{\mathbf{h}}$ defined in (24a). Factor $\|\mathbf{A}(\cdot - \mathbf{x}_{\mathbf{P}}^{\mathbf{k}})\|_{L^{\infty}_{\#}(\Omega_{\mathbf{h}}; \mathbb{R}^{d \times d})}$ then indicates the largest eigenvalue of material coefficients $\mathbf{A}(\mathbf{x}) \in \mathbb{R}^{d \times d}$ over a pixel or voxel $(\mathbf{x}_{\mathbf{P}}^{\mathbf{k}} + \Omega_{\mathbf{h}})$ located at the corresponding grid point $\mathbf{x}_{\mathbf{P}}^{\mathbf{k}}$.

Remark 26. The previous approximation of material coefficients, according to Lemma 24, leads to guaranteed bounds. The following approximation with piece-wise bilinear functions

$$\mathbf{A}(\mathbf{x}) \approx \sum_{\mathbf{k} \in \mathbb{Z}_{\mathbf{P}}^d} \text{tri}_{\mathbf{h}}(\mathbf{x} - \mathbf{x}_{\mathbf{P}}^{\mathbf{k}}) \mathbf{A}(\mathbf{x}_{\mathbf{P}}^{\mathbf{k}}) \quad \text{for } h_{\alpha} = \frac{Y_{\alpha}}{P_{\alpha}}$$

enables the closed-form calculation of bilinear forms; however, the guaranteed bounds are only approximated.

5 Fully discrete formulations and computational aspects

This section is dedicated to reformulating the discretized homogenized problems (18) and (19) into a fully discrete setting which is suitable for computer implementation. Using isometric isomorphism $\mathcal{I}_{\mathbf{N}} : \mathcal{T}_{\mathbf{N}}^d \rightarrow \mathbb{R}^{d \times N}$ defined in (59), the trigonometric polynomials are evaluated at grid points leading to their representation by vectors.

Then, the fully discrete formulations of the GaNi and Ga schemes are derived and stated in sections 5.1 and 5.2; the resolution of corresponding linear systems is discussed in section 5.3. Finally, section 5.4 contains useful information about computational aspects.

5.1 Galerkin approximation with numerical integration

A fully discrete version of GaNi (19) has been introduced in [22, Lemma 5.1] for the odd grids (17) and generalized in [9, Lemma 30] for the general grids and the primal-dual setting. Here, the latter lemma is repeated without proof, which is, however, the direct consequence of Lemma 45 (ii).

Lemma 27. *Using the assumptions of Def. 12, the bilinear forms yield*

$$\begin{aligned}\tilde{a}_N(\mathbf{u}_N, \mathbf{v}_N) &= \tilde{\mathbf{a}}_N(\mathbf{u}_N, \mathbf{v}_N) := (\mathbf{A}_N \mathbf{u}_N, \mathbf{v}_N)_{\mathbb{R}^{d \times N}} \\ \tilde{a}_N^{-1}(\mathbf{u}_N, \mathbf{v}_N) &= \tilde{\mathbf{a}}_N^{-1}(\mathbf{u}_N, \mathbf{v}_N) := (\mathbf{B}_N \mathbf{u}_N, \mathbf{v}_N)_{\mathbb{R}^{d \times N}}\end{aligned}$$

where

$$\mathbf{u}_N := \mathcal{I}_N[\mathbf{u}_N] \in \mathbb{R}^{d \times N} \qquad \mathbf{v}_N := \mathcal{I}_N[\mathbf{v}_N] \in \mathbb{R}^{d \times N}$$

and matrices $\mathbf{A}_N, \mathbf{B}_N \in [\mathbb{R}^{d \times N}]^2$ are defined through their components

$$\mathbf{A}_N^{mk} = \mathbf{A}(\mathbf{x}_N^m) \delta_{mk} \qquad \mathbf{B}_N^{mk} = \mathbf{A}^{-1}(\mathbf{x}_N^m) \delta_{mk}$$

for $\mathbf{m}, \mathbf{k} \in \mathbb{Z}_N^d$; moreover

$$\mathbf{A}_N = \mathbf{B}_N^{-1}. \tag{34}$$

The previous lemma allows us to define of the homogenization problem in a fully discrete setting that represents the matrix-like formulation of GaNi.

Corollary 28 (Fully discrete formulations of the GaNi). *Under the assumptions of Def. 12, the primal and the dual homogenized matrices $\tilde{\mathbf{A}}_{H,N}^{\text{GaNi}}, \tilde{\mathbf{B}}_{H,N}^{\text{GaNi}} \in \mathbb{R}^{d \times d}$ satisfy*

$$\left(\tilde{\mathbf{A}}_{H,N}^{\text{GaNi}} \mathbf{E}, \mathbf{E} \right)_{\mathbb{R}^d} = \inf_{\mathbf{e}_N \in \mathbf{e}_N} \tilde{\mathbf{a}}_N(\mathbf{E} + \mathbf{e}_N, \mathbf{E} + \mathbf{e}_N) = \tilde{\mathbf{a}}_N(\mathbf{E} + \tilde{\mathbf{e}}_N^{(\mathbf{E})}, \mathbf{E} + \tilde{\mathbf{e}}_N^{(\mathbf{E})}) \tag{35a}$$

$$\left(\tilde{\mathbf{B}}_{H,N}^{\text{GaNi}} \mathbf{J}, \mathbf{J} \right)_{\mathbb{R}^d} = \inf_{\mathbf{j}_N \in \mathbf{j}_N} \tilde{\mathbf{a}}_N^{-1}(\mathbf{J} + \mathbf{j}_N, \mathbf{J} + \mathbf{j}_N) = \tilde{\mathbf{a}}_N^{-1}(\mathbf{J} + \tilde{\mathbf{j}}_N^{(\mathbf{J})}, \mathbf{J} + \tilde{\mathbf{j}}_N^{(\mathbf{J})}) \tag{35b}$$

for arbitrary quantities $\mathbf{E}, \mathbf{J} \in \mathbb{R}^d$.

Moreover, discrete minimizers $\tilde{\mathbf{e}}_N^{(\mathbf{E})}, \tilde{\mathbf{j}}_N^{(\mathbf{J})}$ and $\tilde{\mathbf{e}}_N^{(\mathbf{E})}, \tilde{\mathbf{j}}_N^{(\mathbf{J})}$ of both formulations (19) and (35) exist, are unique, and are connected to each other by

$$\mathcal{I}_N[\tilde{\mathbf{e}}_N^{(\mathbf{E})}] = \tilde{\mathbf{e}}_N^{(\mathbf{E})}, \qquad \mathcal{I}_N[\tilde{\mathbf{j}}_N^{(\mathbf{J})}] = \tilde{\mathbf{j}}_N^{(\mathbf{J})}.$$

Remark 29. *The discrete bilinear forms $\tilde{\mathbf{a}}_N, \tilde{\mathbf{a}}_N^{-1}$ are defined on $\mathbb{R}^{d \times N} \times \mathbb{R}^{d \times N}$, rendering the terms $\mathbf{E} + \mathbf{e}_N$ and $\mathbf{J} + \mathbf{j}_N$ formally ill-defined. The sums need to be understood with the help of the isometric isomorphism \mathcal{I}_N from (59) that identifies \mathbb{R}^d or \mathcal{U} with \cup_N , e.g.*

$$\tilde{\mathbf{a}}_N(\mathbf{E} + \mathbf{e}_N, \mathbf{E} + \mathbf{e}_N) = \tilde{\mathbf{a}}_N(\mathcal{I}_N[\mathbf{E}] + \mathbf{e}_N, \mathcal{I}_N[\mathbf{E}] + \mathbf{e}_N) \quad \text{with } (\mathcal{I}_N[\mathbf{E}] + \mathbf{e}_N)_\alpha^k = E_\alpha + \mathbf{e}_{N,\alpha}^k.$$

5.2 Galerkin approximations

The results in section 4 allow to introduce fully discrete versions of bilinear forms (14).

Lemma 30 (Fully discrete bilinear forms of the Ga). *Let N be an approximation order of trigonometric polynomials satisfying the odd grid assumption (17) and*

$$\mathbf{M} \text{ equals one of } (2N - 1), 2N, \text{ or } N. \tag{36}$$

Then, bilinear forms (14) defined on $\mathcal{T}_N^d \times \mathcal{T}_N^d$ allow expression of four discrete versions.

(i) For $\mathbf{a}_M, \mathbf{a}_M^{-1} : \mathbb{R}^{d \times M} \times \mathbb{R}^{d \times M} \rightarrow \mathbb{R}^d$, it holds

$$a(\mathbf{u}_N, \mathbf{v}_N) = \mathbf{a}_M(\mathbf{u}_N, \mathbf{v}_N) := (\mathbf{A}_M^{\text{Ga}} \mathbf{u}_N, \mathbf{v}_N)_{\mathbb{R}^{d \times M}}, \quad (37a)$$

$$a^{-1}(\mathbf{u}_N, \mathbf{v}_N) = \mathbf{a}_M^{-1}(\mathbf{u}_N, \mathbf{v}_N) := (\mathbf{B}_M^{\text{Ga}} \mathbf{u}_N, \mathbf{v}_N)_{\mathbb{R}^{d \times M}}, \quad (37b)$$

where the vectors equal to $\mathbf{u}_N = \mathcal{I}_M[\mathbf{u}_N]$, $\mathbf{v}_N = \mathcal{I}_M[\mathbf{v}_N] \in \mathbb{R}^{d \times M}$, and the matrices $\mathbf{A}_M^{\text{Ga}}, \mathbf{B}_M^{\text{Ga}} \in [\mathbb{R}^{d \times M}]^2$ are defined with regard to (36) as (23), (29), or (30a) respectively.

(ii) For $\widehat{\mathbf{a}}_N, \widehat{\mathbf{a}}_N^{-1} : \mathbb{C}^{d \times N} \times \mathbb{C}^{d \times N} \rightarrow \mathbb{C}^d$, it holds

$$a(\mathbf{u}_N, \mathbf{v}_N) = \widehat{\mathbf{a}}_N(\widehat{\mathbf{u}}_N, \widehat{\mathbf{v}}_N) := (\widehat{\mathbf{A}}_N^{\text{Ga}} \widehat{\mathbf{u}}_N, \widehat{\mathbf{v}}_N)_{\mathbb{C}^{d \times N}},$$

$$a^{-1}(\mathbf{u}_N, \mathbf{v}_N) = \widehat{\mathbf{a}}_N^{-1}(\widehat{\mathbf{u}}_N, \widehat{\mathbf{v}}_N) := (\widehat{\mathbf{B}}_N^{\text{Ga}} \widehat{\mathbf{u}}_N, \widehat{\mathbf{v}}_N)_{\mathbb{C}^{d \times N}}.$$

for vectors $\widehat{\mathbf{u}}_N = \mathbf{F}_N \mathcal{I}_N[\mathbf{u}_N]$, $\widehat{\mathbf{v}}_N = \mathbf{F}_N \mathcal{I}_N[\mathbf{v}_N] \in \mathbb{C}^{d \times N}$, and matrices $\widehat{\mathbf{A}}_N^{\text{Ga}}, \widehat{\mathbf{B}}_N^{\text{Ga}} \in [\mathbb{C}^{d \times N}]^2$ defined according to (30b).

Proof. It is a direct consequence of Lemmas 16, 21, and Eq. (22). \square

Remark 31. The sparse quadrature on a double grid involves the projection to a finer grid denoted as

$$\mathbf{u}_N = \mathcal{I}_M[\mathbf{u}_N] \in \mathbb{R}^{d \times M} \quad \text{for } M, N \in \mathbb{R}^d \text{ such that } M_\alpha > N_\alpha. \quad (38)$$

The symbol N is consistently used for the approximation order of trigonometric polynomials \mathcal{T}_N^d while symbol M in (36) is used for the grid size in accordance with the type of numerical integration. In (38), the author decided to use the same subscript N for the trigonometric polynomial \mathbf{u}_N and its discrete representation \mathbf{u}_N in order to highlight their polynomial degree and to avoid a profusion of notation. The actual dimension of \mathbf{u}_N is understood implicitly from the context, so that terms such as $\mathbf{a}_M(\mathbf{u}_N, \mathbf{u}_N)$ or $(\mathbf{A}_M \mathbf{u}_N, \mathbf{u}_N)_{\mathbb{R}^{d \times M}}$ with $\mathbf{A}_M \in [\mathbb{R}^{d \times M}]^2$ remain well-defined.

For the need of fully discrete formulation of the Ga scheme (18), the author defines the spaces of vectors

$$\mathbb{E}_{N,M} = \mathcal{I}_M[\mathcal{E}_N] \subset \mathbb{R}^{d \times M}, \quad \mathbb{J}_{N,M} = \mathcal{I}_M[\mathcal{J}_N] \subset \mathbb{R}^{d \times M}, \quad (39a)$$

$$\widehat{\mathbb{E}}_N = \mathbf{F}_N[\mathbb{E}_N] \subset \mathbb{C}^{d \times N}, \quad \widehat{\mathbb{J}}_N = \mathbf{F}_N[\mathbb{J}_N] \subset \mathbb{C}^{d \times N}, \quad (39b)$$

which are generalizations of those in Definition 48. The subspaces coincide $\mathbb{E}_N = \mathbb{E}_{N,M}$, $\mathbb{J}_N = \mathbb{J}_{N,M}$ for $N = M$ and their relation to the trigonometric polynomials and to the spaces of Helmholtz decomposition are depicted in Figure 11. Otherwise, the discretization complies with the strategy in Figure 2.

$$\begin{array}{ccccc}
\mathcal{J} & \xrightarrow{p_N} & \mathcal{J}_N & \xrightarrow{\mathcal{I}_M} & \mathbb{J}_{N,M} \\
\mathcal{G} \uparrow & & \mathcal{G} \uparrow & & \mathcal{G}_{N,M} \uparrow \\
L^2_{\text{per}}(\mathcal{Y}; \mathbb{R}^d) & \xrightarrow{p_N} & \mathcal{T}_N^d & \xrightarrow{\mathcal{I}_M} & \mathcal{I}_M[\mathcal{T}_N^d] \subseteq \mathbb{R}^{d \times M} \\
\mathcal{G} \downarrow & & \mathcal{G} \downarrow & & \mathcal{G}_{N,M} \downarrow \\
\mathcal{E} & \xrightarrow{p_N} & \mathcal{E}_N & \xrightarrow{\mathcal{I}_M} & \mathbb{E}_{N,M}
\end{array}$$

Figure 2: Discretization strategy for $N, M \in \mathbb{N}^d$ such that $N_\alpha \leq M_\alpha$

Corollary 32 (Fully discrete formulations of Ga). *Let $\mathbf{N} \in \mathbb{R}^d$ and $\mathbf{M} \in \mathbb{R}^d$ satisfy odd grid assumptions (17) and (36), respectively. Then for the discrete bilinear forms from previous Lemma 30 and subspaces from (39), the primal and the dual homogenized matrices $\mathbf{A}_{\text{H},\mathbf{N}}, \mathbf{B}_{\text{H},\mathbf{N}} \in \mathbb{R}^{d \times d}$ of the Ga scheme (18) satisfy*

$$(\mathbf{A}_{\text{H},\mathbf{N}}\mathbf{E}, \mathbf{E})_{\mathbb{R}^d} = \inf_{\mathbf{e}_N \in \mathcal{E}_{\mathbf{N},\mathbf{M}}} \mathbf{a}_M(\mathbf{E} + \mathbf{e}_N, \mathbf{E} + \mathbf{e}_N) = \mathbf{a}_M(\mathbf{E} + \mathbf{e}_N^{(\mathbf{E})}, \mathbf{E} + \mathbf{e}_N^{(\mathbf{E})}) \quad (40a)$$

$$= \inf_{\hat{\mathbf{e}}_N \in \hat{\mathcal{E}}_N} \hat{\mathbf{a}}_N(\hat{\mathbf{E}} + \hat{\mathbf{e}}_N, \hat{\mathbf{E}} + \hat{\mathbf{e}}_N) = \hat{\mathbf{a}}_N(\hat{\mathbf{E}} + \hat{\mathbf{e}}_N^{(\mathbf{E})}, \hat{\mathbf{E}} + \hat{\mathbf{e}}_N^{(\mathbf{E})}), \quad (40b)$$

$$(\mathbf{B}_{\text{H},\mathbf{N}}\mathbf{J}, \mathbf{J})_{\mathbb{R}^d} = \inf_{\mathbf{j}_N \in \mathcal{J}_{\mathbf{N},\mathbf{M}}} \mathbf{a}_M^{-1}(\mathbf{J} + \mathbf{j}_N, \mathbf{J} + \mathbf{j}_N) = \mathbf{a}_M^{-1}(\mathbf{J} + \mathbf{j}_N^{(\mathbf{J})}, \mathbf{J} + \mathbf{j}_N^{(\mathbf{J})}) \quad (40c)$$

$$= \inf_{\hat{\mathbf{j}}_N \in \hat{\mathcal{J}}_N} \hat{\mathbf{a}}_N^{-1}(\hat{\mathbf{J}} + \hat{\mathbf{j}}_N, \hat{\mathbf{J}} + \hat{\mathbf{j}}_N) = \hat{\mathbf{a}}_N^{-1}(\hat{\mathbf{J}} + \hat{\mathbf{j}}_N^{(\mathbf{J})}, \hat{\mathbf{J}} + \hat{\mathbf{j}}_N^{(\mathbf{J})}), \quad (40d)$$

for arbitrary quantities $\mathbf{E}, \mathbf{J} \in \mathbb{R}^d$, where $\hat{\mathbf{E}} = \mathbf{F}_N \mathcal{I}_N[\mathbf{E}]$ and $\hat{\mathbf{J}} = \mathbf{F}_N \mathcal{I}_N[\mathbf{J}]$. Moreover, the minimizers $\mathbf{e}_N^{(\mathbf{E})} \in \mathcal{E}_N$ and $\mathbf{j}_N^{(\mathbf{J})} \in \mathcal{J}_N$ are related to $\mathbf{e}_N^{(\mathbf{E})}, \mathbf{j}_N^{(\mathbf{J})} \in \mathbb{R}^{d \times M}$ and $\hat{\mathbf{e}}_N^{(\mathbf{E})}, \hat{\mathbf{j}}_N^{(\mathbf{J})} \in \mathbb{C}^{d \times M}$ introduced in (40) according to

$$\mathbf{e}_N^{(\mathbf{E})} = \mathcal{I}_M^{-1}[\mathbf{e}_N^{(\mathbf{E})}] = \mathcal{I}_N^{-1}[\mathbf{F}_N^{-1}\hat{\mathbf{e}}_N^{(\mathbf{E})}], \quad \mathbf{j}_N^{(\mathbf{J})} = \mathcal{I}_M^{-1}[\mathbf{j}_N^{(\mathbf{J})}] = \mathcal{I}_N^{-1}[\mathbf{F}_N^{-1}\hat{\mathbf{j}}_N^{(\mathbf{J})}]. \quad (41)$$

Proof of Corollary 32. This is a direct consequence of Definition 10 and Lemmas 16, 21, and (22). \square

5.3 Linear systems

This section deals with solutions of linear systems derived from fully discrete formulations. This topic has already been studied in [22, section 5] and [9, section 7] for the GaNi scheme (19). Here, the concept is summarized and extended to the Ga scheme (18).

Proposition 33 (From minimization to linear system). *Let \mathcal{H} be a Hilbert space with a non-trivial orthogonal decomposition $\mathcal{H} = \mathcal{U} \oplus \mathcal{E} \oplus \mathcal{J}$, where \mathcal{U} is isometrically isomorphic with \mathbb{R}^d . Next, let bilinear form $\mathring{a} : \mathcal{H} \times \mathcal{H} \rightarrow \mathbb{R}$ be defined as*

$$\mathring{a}(\mathbf{u}, \mathbf{v}) = (\mathring{\mathbf{A}}\mathbf{u}, \mathbf{v})_{\mathcal{H}},$$

for the symmetric, coercive, and bounded linear operator $\mathring{\mathbf{A}} : \mathcal{H} \rightarrow \mathcal{H}$ so that there are $c_{\mathring{\mathbf{A}}} > 0$ and $C_{\mathring{\mathbf{A}}} > 0$ such that

$$c_{\mathring{\mathbf{A}}}\|\mathbf{u}\|_{\mathcal{H}} \leq (\mathring{\mathbf{A}}\mathbf{u}, \mathbf{u})_{\mathcal{H}} \leq C_{\mathring{\mathbf{A}}}\|\mathbf{u}\|_{\mathcal{H}} \quad \text{for all } \mathbf{u} \in \mathcal{H}.$$

Then a problem for $\mathbf{E} \in \mathcal{U}$ to find a minimizer $\mathring{\mathbf{e}}^{(\mathbf{E})} \in \mathcal{E}$ of

$$\mathring{\mathbf{e}}^{(\mathbf{E})} = \arg \min_{\mathring{\mathbf{e}} \in \mathcal{E}} \mathring{a}(\mathbf{E} + \mathring{\mathbf{e}}, \mathbf{E} + \mathring{\mathbf{e}}) \quad (42)$$

is equivalent to finding the solution $\mathring{\mathbf{e}}^{(\mathbf{E})} \in \mathcal{E}$ of the following equation in \mathcal{H}

$$\mathring{\mathbf{G}}\mathring{\mathbf{A}}\mathring{\mathbf{e}}^{(\mathbf{E})} = -\mathring{\mathbf{G}}\mathring{\mathbf{A}}\mathbf{E}, \quad (43)$$

where $\mathring{\mathbf{G}}$ is an orthogonal projection on \mathcal{E} .

Proof. The proof starts with an optimality condition of (42), namely

$$\dot{a}(\dot{e}_N^{(E)}, \mathbf{v}) = -\dot{a}(\mathbf{E}, \mathbf{v}) \quad \forall \mathbf{v} \in \mathcal{E}.$$

Then, the projection is incorporated in order to enlarge the space of test functions

$$\begin{aligned} \dot{a}(\dot{e}_N^{(E)}, \dot{\mathbf{G}}\mathbf{v}) &= -\dot{a}(\mathbf{E}, \dot{\mathbf{G}}\mathbf{v}) \quad \forall \mathbf{v} \in \mathcal{H}, \\ (\dot{\mathbf{G}}\dot{\mathbf{A}}\dot{e}_N^{(E)}, \mathbf{v})_{\mathcal{H}} &= -(\dot{\mathbf{G}}\dot{\mathbf{A}}\mathbf{E}, \mathbf{v})_{\mathcal{H}} \quad \forall \mathbf{v} \in \mathcal{H}, \end{aligned}$$

where the orthogonality (symmetry) of $\dot{\mathbf{G}}$ has also been used. Now, it is possible to remove the scalar product and deduce the required (43). \square

Corollary 34 (Linear systems for the GaNi). *The minimizers $\tilde{\mathbf{e}}_N^{(E)} \in \mathbb{E}_N$ and $\tilde{\mathbf{j}}_N^{(J)} \in \mathbb{J}_N$ for $\mathbf{E}, \mathbf{J} \in \mathbb{R}^d$ in fully discrete formulation of the GaNi scheme (35) satisfy the following equations*

$$\mathbf{G}_N^{\mathcal{E}} \mathbf{A}_N \tilde{\mathbf{e}}_N^{(E)} = -\mathbf{G}_N^{\mathcal{E}} \mathbf{A}_N \mathbf{E}, \quad \mathbf{G}_N^{\mathcal{J}} \mathbf{A}_N^{-1} \tilde{\mathbf{j}}_N^{(J)} = -\mathbf{G}_N^{\mathcal{J}} \mathbf{A}_N^{-1} \mathbf{J}.$$

The application of the previous lemma to the Ga scheme (40) requires projections onto relating subspaces; for this purpose, the following definition and lemma are introduced.

Definition 35. *Let $N \in \mathbb{R}^d$ satisfy the odd grid assumption (17), $M \in \mathbb{R}^d$ be a vector such that $N_\alpha < M_\alpha$ for all α , $\widehat{\mathbb{E}}_N, \widehat{\mathbb{J}}_N$ be subsets of $\mathbb{C}^{d \times N}$ from (39b), and $\mathbb{E}_{N,M}, \mathbb{J}_{N,M}$ be subsets of $\mathbb{R}^{d \times M}$ from (39a).*

Then matrices $\widehat{\mathbf{G}}_{N,M}^{\mathcal{E}}, \widehat{\mathbf{G}}_{N,M}^{\mathcal{J}} \in [\mathbb{R}^{d \times M}]^2$ are defined as

$$\left(\widehat{\mathbf{G}}_{N,M}^{\mathcal{E}}\right)^{kl} = \begin{cases} \widehat{\mathbf{G}}_N^{\mathcal{E},kl} & \text{for } \mathbf{k}, \mathbf{l} \in \mathbb{Z}_N^d, \\ \mathbf{0} & \text{otherwise} \end{cases}, \quad \left(\widehat{\mathbf{G}}_{N,M}^{\mathcal{J}}\right)^{kl} = \begin{cases} \widehat{\mathbf{G}}_N^{\mathcal{J},kl} & \text{for } \mathbf{k}, \mathbf{l} \in \mathbb{Z}_N^d, \\ \mathbf{0} & \text{otherwise} \end{cases}, \quad (44a)$$

where the matrices $\widehat{\mathbf{G}}_N^{\mathcal{E}}, \widehat{\mathbf{G}}_N^{\mathcal{J}}$, are introduced in Definition 46. Next, matrices $\mathbf{G}_{N,M}^{\mathcal{E}}, \mathbf{G}_{N,M}^{\mathcal{J}} \in [\mathbb{R}^{d \times M}]^2$ are defined as

$$\mathbf{G}_{N,M}^{\mathcal{E}} = \mathbf{F}_M^{-1} \widehat{\mathbf{G}}_{N,M}^{\mathcal{E}} \mathbf{F}_M, \quad \mathbf{G}_{N,M}^{\mathcal{J}} = \mathbf{F}_M^{-1} \widehat{\mathbf{G}}_{N,M}^{\mathcal{J}} \mathbf{F}_M, \quad (44b)$$

where the DFT matrices $\mathbf{F}_M, \mathbf{F}_M^{-1} \in [\mathbb{C}^{d \times M}]^2$ are defined in (58).

Lemma 36 (Discrete projections). *Operators $\widehat{\mathbf{G}}_N^{\mathcal{E}}, \widehat{\mathbf{G}}_N^{\mathcal{J}} : \mathbb{C}^{d \times N} \rightarrow \mathbb{C}^{d \times N}$ are projections on $\widehat{\mathbb{E}}_N, \widehat{\mathbb{J}}_N$ and operators $\mathbf{G}_{N,M}^{\mathcal{E}}, \mathbf{G}_{N,M}^{\mathcal{J}} : \mathbb{R}^{d \times M} \rightarrow \mathbb{R}^{d \times M}$ are projections on $\mathbb{E}_{N,M}, \mathbb{J}_{N,M}$, respectively.*

Proof. Because of the analogy, the proof addresses only the primal operators. Indeed, $\widehat{\mathbf{G}}_N^{\mathcal{E}}$ is a projection on $\widehat{\mathbb{E}}_N = \mathbf{F}[\mathbb{E}_N]$ thanks to its construction in Definition 46. Then operator $\widehat{\mathbf{G}}_{N,M}^{\mathcal{E}}$ is a projection on $\mathbf{F}_M[\mathbb{E}_{N,M}]$ because of the zero Fourier coefficients for frequencies $\mathbf{k} \in \mathbb{Z}_M^d \setminus \mathbb{Z}_N^d$ in the matrix $\widehat{\mathbf{G}}_{N,M}^{\mathcal{E}}$ and also in any vector $\mathbf{u}_N \in \mathbb{E}_{N,M}$, i.e.

$$\widehat{\mathbf{u}}_N^{\mathbf{k}} = (\mathbf{F}_M \mathbf{u}_N)^{\mathbf{k}} = \mathbf{0} \quad \text{for } \mathbf{k} \in \mathbb{Z}_M^d \setminus \mathbb{Z}_N^d$$

following (39) and Definition 48. Using the same argumentation, operator $\mathbf{G}_{N,M}^{\mathcal{E}}$ is a projection on $\mathbb{E}_{N,M}$. \square

Using Proposition 33 and the discrete projections from the previous lemma result in linear systems corresponding to the Ga scheme.

Corollary 37 (Linear systems for the Ga). *Using the assumptions from Corollary 32, the following holds for minimizers in (40).*

(i) *The minimizers $\mathbf{e}_N^{(\mathbf{E})} \in \mathbb{E}_{N,M}$ and $\mathbf{j}_N^{(\mathbf{J})} \in \mathbb{J}_{N,M}$ for $\mathbf{E}, \mathbf{J} \in \mathbb{R}^d$ satisfy*

$$\mathbf{G}_{N,M}^{\mathcal{E}} \mathbf{A}_M^{\text{Ga}} \mathbf{e}_N^{(\mathbf{E})} = -\mathbf{G}_{N,M}^{\mathcal{E}} \mathbf{A}_M^{\text{Ga}} \mathbf{E}, \quad \mathbf{G}_{N,M}^{\mathcal{J}} \mathbf{B}_M^{\text{Ga}} \mathbf{j}_N^{(\mathbf{J})} = -\mathbf{G}_{N,M}^{\mathcal{J}} \mathbf{B}_M^{\text{Ga}} \mathbf{J}, \quad (45)$$

where the matrices $\mathbf{G}_{N,M}^{\mathcal{E}}, \mathbf{G}_{N,M}^{\mathcal{J}} \in [\mathbb{R}^{d \times M}]^2$ are defined according to Lemma 36 and $\mathbf{A}_M^{\text{Ga}}, \mathbf{B}_M^{\text{Ga}} \in [\mathbb{R}^{d \times M}]^2$ are defined with regard to (36) as (23), (29), or (30a), respectively.

(ii) *The minimizers $\hat{\mathbf{e}}_N^{(\mathbf{E})} \in \hat{\mathbb{E}}_N$ and $\hat{\mathbf{j}}_N^{(\mathbf{J})} \in \hat{\mathbb{J}}_N$ for $\mathbf{E}, \mathbf{J} \in \mathbb{R}^d$ satisfy*

$$\hat{\mathbf{G}}_N^{\mathcal{E}} \hat{\mathbf{A}}_N^{\text{Ga}} \hat{\mathbf{e}}_N^{(\mathbf{E})} = -\hat{\mathbf{G}}_N^{\mathcal{E}} \hat{\mathbf{A}}_N^{\text{Ga}} \hat{\mathbf{E}}, \quad \hat{\mathbf{G}}_N^{\mathcal{J}} \hat{\mathbf{B}}_N^{\text{Ga}} \hat{\mathbf{j}}_N^{(\mathbf{J})} = -\hat{\mathbf{G}}_N^{\mathcal{J}} \hat{\mathbf{B}}_N^{\text{Ga}} \hat{\mathbf{J}}, \quad (46)$$

where $\hat{\mathbf{G}}_N^{\mathcal{E}}, \hat{\mathbf{G}}_N^{\mathcal{J}}$ are defined in (61) and $\hat{\mathbf{A}}_N^{\text{Ga}}, \hat{\mathbf{B}}_N^{\text{Ga}}$ are defined according to (30a).

5.4 Computational and implementation issues

The previous section investigated the connection between discrete minimization problems, see (35) and (40), and their corresponding linear systems. This section focuses on the computational aspects of finding minimizers leading to evaluation of homogenized properties.

Remark 38 (Solution by conjugate gradients). *The discrete problems, see the GaNi (35) and Ga (40) schemes, can be effectively solved with Krylov subspace methods [56, 57], particularly conjugate gradients, which were noticed in [28, 19] and explained by variational reformulation in [23, 22] for the GaNi scheme (35).*

Using the general notation from Proposition 33, the minimization problems of both discrete schemes (35) and (40) rely on the quadratic functional (42). This perfectly employs conjugate gradients (CG) since the minimization over subspace can be carried out with projection matrix $\hat{\mathbf{G}}$ on $\hat{\mathcal{E}}$ introduced in Definition 46 and Equations (44b), (44a).

The minimization process also corresponds to the solution of the linear system (43) with an initial approximation $\hat{\mathbf{e}}_{(0)}^{(\mathbf{E})}$ from the minimization space $\hat{\mathcal{E}}$, which ensures that a residual vector

$$\mathbf{r}_{(k)} = -\hat{\mathbf{G}} \hat{\mathbf{A}} \hat{\mathbf{e}}_{(k)}^{(\mathbf{E})} - \hat{\mathbf{G}} \hat{\mathbf{A}} \mathbf{E}$$

is from the subspace $\hat{\mathcal{E}}$ for arbitrary k -th iteration. Then the CG algorithm is interpreted as a minimization

$$\hat{\mathbf{e}}_{(k)}^{(\mathbf{E})} = \arg \min_{\hat{\mathbf{e}} \in \hat{\mathbf{e}}_{(0)}^{(\mathbf{E})} + \mathbb{K}_{(i)}} \hat{a}(\mathbf{E} + \hat{\mathbf{e}}, \mathbf{E} + \hat{\mathbf{e}})$$

over Krylov subspaces defined for $i = 1, 2, \dots$ as

$$\mathbb{K}_{(i)} = \text{span} \left\{ \mathbf{r}_{(0)}, \hat{\mathbf{G}} \hat{\mathbf{A}} \mathbf{r}_{(0)}, \dots, (\hat{\mathbf{G}} \hat{\mathbf{A}})^{i-1} \mathbf{r}_{(0)} \right\} \quad \text{satisfying } \mathbb{K}_{(i)} \subseteq \mathbb{K}_{(i+1)} \subseteq \hat{\mathcal{E}} = \hat{\mathbf{G}}[\mathcal{H}].$$

The specific linear systems can be found in Lemma 34 for the GaNi scheme and in Lemma 37 for the Ga scheme.

Remark 39 (Evaluation of matrices with FFT). *Matrices (26) and (28) derived for the inclusion-matrix composite (25) and grid-based composites can be evaluated efficiently using the FFT algorithm. For (26), the Fourier coefficients (7) of each inclusion topology $[\hat{f}_{(i)}(\mathbf{m})]^{\mathbf{m} \in \mathbb{Z}_{2\mathbf{N}}^d}$ for $i = 1, \dots, n$ are evaluated and shifted to account for the inclusion position $\hat{\mathbf{x}}$; the shift is expressed*

with element-wise multiplication by matrix $[\varphi_{-\mathbf{m}}(\bar{\mathbf{x}}_{(i)})]^{m \in \mathbb{Z}_{2N}^d}$. Finally, the sum over $\mathbf{k} \in \mathbb{Z}_{2N}^d$ represents multiplication with DFT (58), numerically evaluated with the FFT algorithm.

For (28), the sum over $\mathbb{Z}_{\mathbf{P}}^d$ and \mathbb{Z}_{2N-1}^d is provided by \mathbf{P} -sized FFT and $(2N-1)$ -sized inverse FFT algorithm resp., whereas the factor $\hat{\psi}(\mathbf{m})$ occurs as an element-wise multiplication. However, for $\mathbf{P} \neq 2N-1$, the additional treatment has to be provided. For $P_\alpha > 2N_\alpha - 1$, the vector

$$\left(\sum_{\mathbf{n} \in \mathbb{Z}_{\mathbf{P}}^d} \frac{\omega_{\mathbf{P}}^{-\mathbf{m}\mathbf{n}}}{|\mathbf{P}|} A_{\mathbf{P}, \alpha\beta}^{\mathbf{n}} \right)^{m \in \mathbb{Z}_{\mathbf{P}}^d} \in \mathbb{C}^{\mathbf{P}}$$

is truncated to \mathbb{C}^{2N-1} , while for $P_\alpha < 2N_\alpha - 1$, it is periodically enlarged to \mathbb{C}^{2N-1} thanks to the periodicity of $\omega_{\mathbf{P}}^{\mathbf{n}}$.

Remark 40. In Lemma 22, the fully discrete Ga scheme (40) defined on a double grid has been reformulated to the original grid using shifts of DFT (58). The evaluation of homogenized properties then becomes more memory efficient because the minimizers are stored only on grid sizing N instead of $2N-1$. However, the computational requirements are increased because shift matrices are evaluated (or stored) and the FFT algorithm incorporated. Nevertheless, the computational requirements for the solution of linear system (45) on the double grid are balanced with the reduced system when solved in the Fourier space (46); the FFT algorithm is employed only for shifts to evaluate a material law with matrix (30b) while projection operators in Fourier space (61) remain without the FFT. Specifically, one FFT with size $2N-1$ is substituted for 2^d (corresponding to the number of DFT shifts) with size N .

6 Numerical examples

This section is dedicated to numerical examples that describe the properties of guaranteed bounds (21), especially the homogenized coefficients of Galerkin approximation defined in continuous (18) or discrete settings (40).

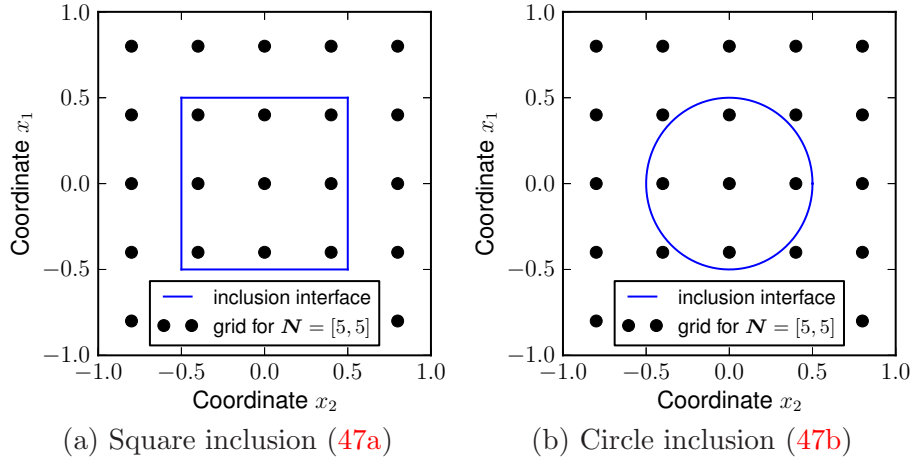


Figure 3: Cells with grid and inclusion interfaces for size $s = \frac{1}{2}$

Problem 41. A two-dimensional problem with material coefficients defined on a periodic cell $\mathcal{Y} = (-1, 1) \times (-1, 1) \subset \mathbb{R}^2$ is considered and defined via

$$\mathbf{A}(\mathbf{x}) = \mathbf{I}[1 + \rho f(\mathbf{x})] \quad \text{for } \mathbf{x} \in \mathcal{Y},$$

where $\mathbf{I} \in \mathbb{R}^{2 \times 2}$ is the identity matrix, $f: \mathcal{Y} \rightarrow \mathbb{R}$ is a scalar nonnegative function which controls the shape of inclusions (recall Remark 17 for specific examples), and $\rho > 0$ is a parameter corresponding to the phase contrast. Two types of inclusions, square and circle, are considered, namely

$$f(\mathbf{x}) = \begin{cases} 1 & \text{for } \|\mathbf{x}\|_\infty < s, \\ 0 & \text{otherwise} \end{cases}, \quad (47a)$$

$$f(\mathbf{x}) = \begin{cases} 1 & \text{for } \|\mathbf{x}\|_2 < s, \\ 0 & \text{otherwise} \end{cases}, \quad (47b)$$

where parameter s corresponds to an inclusion size. The problem is discretized with odd grids (17) with an example shown in Figure 3 along with inclusion interfaces for both geometries (47).

Remark 42. All the calculations have been provided using Python software *FFTHomPy* available at: <https://github.com/vondrejck/FFTHomPy.git>. The linear systems presented in section 5.3 have been solved by conjugate gradients; a convergence criterion on the norm of residuum has been chosen with a relatively small tolerance 10^{-6} in order to suppress algebraic error.

The numerical examples are separated into the following parts: section 6.1 explores sensitivity of homogenized properties in regard to inclusion size, section 6.2 describes an evolution of upper-lower bounds for an increase in grid points, section 6.3 treats the behavior with different phase contrasts, and section 6.4 shows the progress of guaranteed bounds during iterations of conjugate gradients.

6.1 Numerical sensitivity for the inclusion size

Here, homogenized properties are investigated with regard to an inclusion size s . Figure 4 depicts the results for a relatively small number of discretization points $\mathbf{N} = (5, 5)$ which highlight the difference between the Ga (18) and GaNi (19) schemes.

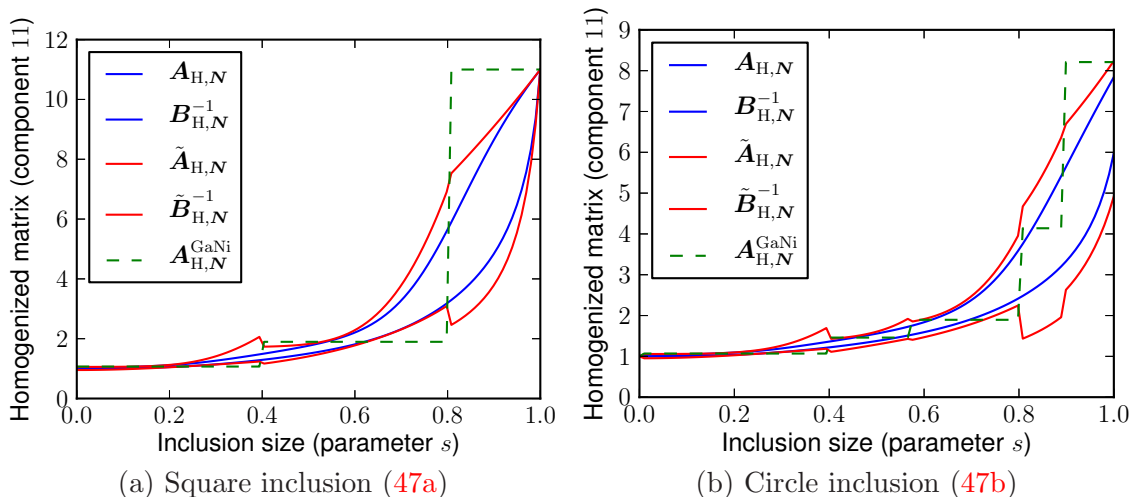


Figure 4: Sensitivity of homogenized properties for $\rho = 10$ and $\mathbf{N} = (5, 5)$

The structure in (21) is satisfied, with better results obtained for homogenized coefficients $\mathbf{A}_{H,N}, \mathbf{B}_{H,N}^{-1}$ using the Ga scheme (18) when compared to the guaranteed bounds $\tilde{\mathbf{A}}_{H,N}, \tilde{\mathbf{B}}_{H,N}^{-1}$ of the GaNi (20). The GaNi matrix $\mathbf{A}_{H,N}^{\text{GaNi}}$ in (19) together with its guaranteed bounds (20) has

already been studied in [9], where the authors point out that the homogenized matrix $\mathbf{A}_{\text{H},N}^{\text{GaNi}}$, in some cases, underestimates or overestimates its own guaranteed bounds $\tilde{\mathbf{A}}_{\text{H},N}$ and $\tilde{\mathbf{B}}_{\text{H},N}^{-1}$, respectively. This GaNi scheme (19) is influenced by inaccurate numerical integration which disregards exact inclusion shapes because the scheme is defined only on grid points. As a result of exact integration, the homogenized matrices $\mathbf{A}_{\text{H},N}$, $\mathbf{B}_{\text{H},N}$ change smoothly in relation to the inclusion size s .

6.2 Upper-lower bounds for an increase in the number of grid points

This section is dedicated to the behavior of homogenized properties for an increase in the number of discretization points N satisfying the odd grid assumption (17). It is depicted in Figures 5 and 6 for homogenized properties and also for normalized errors defined as

$$\eta_N := \frac{\text{tr } \mathbf{D}_N}{\text{tr } \underline{\mathbf{A}}_{\text{H},M}}, \quad \tilde{\eta}_N := \frac{\text{tr } \tilde{\mathbf{D}}_N}{\text{tr } \underline{\mathbf{A}}_{\text{H},M}} \quad (48)$$

where $M = (145, 145)$ and

$$\mathbf{D}_N := \frac{\mathbf{A}_{\text{H},N} - \mathbf{B}_{\text{H},N}^{-1}}{2}, \quad \tilde{\mathbf{D}}_N := \frac{\tilde{\mathbf{A}}_{\text{H},N} - \tilde{\mathbf{B}}_{\text{H},N}^{-1}}{2}, \quad \underline{\mathbf{A}}_{\text{H},M} := \frac{\mathbf{A}_{\text{H},M} + \mathbf{B}_{\text{H},M}^{-1}}{2}.$$

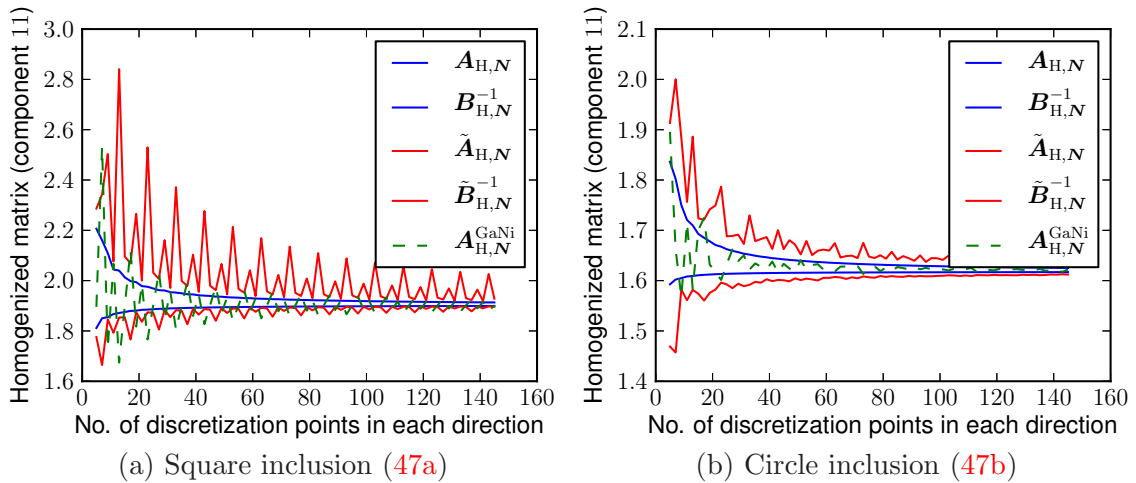


Figure 5: Bounds on homogenized matrix for inclusion size $s = 0.6$ and phase contrast $\rho = 10$

All the homogenized coefficients from both the Ga and GaNi schemes support the structure of guaranteed bounds (21) and converge to homogenized matrix \mathbf{A}_{H} for an increasing number of grid points, which has been proven theoretically in [22, section 4.2 and 4.3]. Thanks to the hierarchy of approximation spaces

$$\mathcal{E}_N \subseteq \mathcal{E}_M \subseteq \mathcal{E} \quad \text{and} \quad \mathcal{I}_N \subseteq \mathcal{I}_M \subseteq \mathcal{I} \quad \text{for } N_\alpha \leq M_\alpha, \quad (49)$$

the homogenized matrices of the Ga scheme $\mathbf{A}_{\text{H},N}$, $\mathbf{B}_{\text{H},N}^{-1}$ evolve monotonically as opposed to the homogenized matrices of the GaNi scheme, which suffer, as already noticed in previous section, from inexact numerical integration causing the so-called "variational crime" [58].

The normalized errors, introduced and studied in [45] for the Finite Element Method, develop in the same rate for both schemes and this confirms the theoretical results regarding the convergence of minimizers presented in [22, section 4.2 and 4.3] for FFT-based methods. Moreover, errors in the Ga scheme evolve almost as a straight line and this allows us to predict the

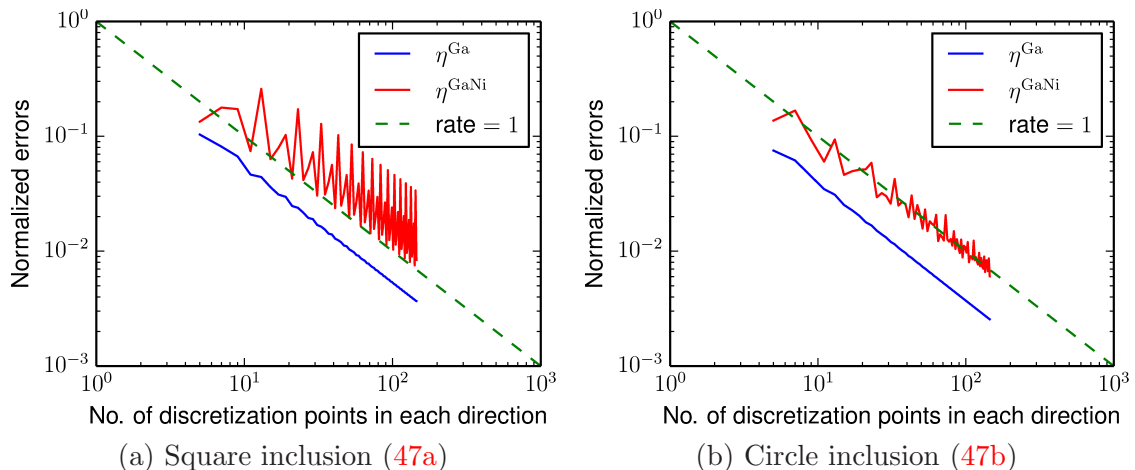


Figure 6: Normalized errors for inclusion size $s = 0.6$ and phase contrast $\rho = 10^1$

number of grid points required to achieve the necessary accuracy. Finally, both the homogenized properties of the GaNi and the normalized error undergo more zigzag behavior for square (47a) than for circle inclusion (47b), because the material coefficients change at all grid points along the square interface for a change in its size or in the number of grid points.

6.3 The progress of normalized errors for increase in phase ratio

This section investigates the homogenized properties in terms of normalized errors (48) for an increase in phase contrast ρ (see Figure 7). The Ga (10) is superior to the GaNi (19) with approximate rates $\frac{1}{2}$ and 1, respectively. These rates scarcely depend on the inclusion shape and the number of grid points; however, they are influenced by round-off errors occurring in conjugate gradients for higher values of phase contrast ρ , which results in the higher condition numbers of linear systems presented in section 5.3.

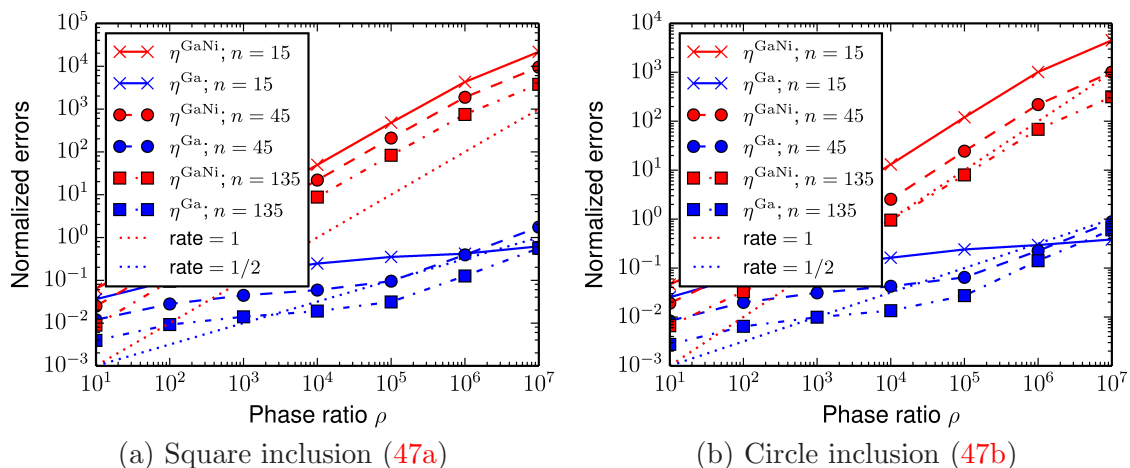


Figure 7: Normalized errors for increase in phase contrast ρ ; $s = 0.6$, $\mathbf{N} = [n, n]$

6.4 The evolution of guaranteed bounds during iterations of conjugate gradients

Here, the author investigates the evolution of bounds during iterations of conjugate gradients (CG). In each iteration, a guaranteed bound corresponding to the energetic norm of the fully

discrete formulation (40) is evaluated. The results are shown in Figure 8 for primal formulation (upper bound), both topologies, and a relatively high phase contrast $\rho = 10^4$ to highlight the behavior.

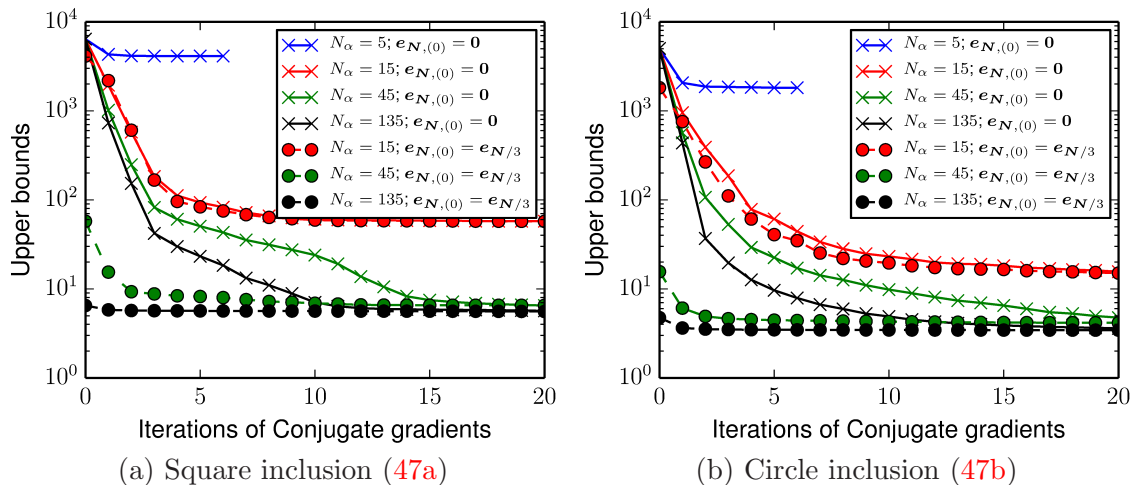


Figure 8: Upper bounds during iterations of conjugate gradients; $\rho = 10^4$; $s = 0.8$

According to the standard results summarized in Remark 38, CG minimize the quadratic functional corresponding to the upper bound; the monotonic evolution of homogenized properties is confirmed in Figure 8. For all grid sizes, since the initial approximation for CG is taken as a zero vector, the bounds begin from a Voigt bound $\langle \mathbf{A} \rangle$, the mean of material coefficients. This starting point can be significantly improved using a hierarchy of approximation spaces (49) in accordance to the p-version of the FEM [45] when a solution on a coarse grid is used as an initial approximation on a fine grid, for example a first vector $\mathbf{e}_{N,(0)}$ for $\mathbf{N} = [45, 45]$ is taken as the solution $\mathbf{e}_{N/3}$ for $\mathbf{N}/3 = [15, 15]$.

6.5 Fly ash foam

Here, the author shows how these methods can be applied to a complex material consisting of alkali-activated fly ash foam. The coefficients, according to [59],

$$\mathbf{A}(\mathbf{x}) = [0.49 \cdot f(\mathbf{x}) + 0.029 \cdot (1 - f(\mathbf{x}))] \cdot \mathbf{I} \quad \text{for } \mathbf{x} \in \mathcal{Y},$$

are defined via a fly ash phase characteristic function $f : \mathcal{Y} \rightarrow \mathbb{R}$ depicted in Figure 9 as a voxel-based image with resolution $\mathbf{N} = [99, 99, 99]$ corresponding to 970299 points.

The models were calculated on a conventional laptop (Intel®Core™i5-4200M CPU @ 2.5 GHz \times 2 processor and 8 GB of RAM) within less than an hour for both the GaNi and the Ga schemes. The results are represented for eigenvalues of homogenized coefficients because they also satisfy the structure of upper-lower bounds (21), i.e. for the Ga scheme (18)

$$\text{eig } \mathbf{A}_{H,N} = [0.12910304 \quad 0.13832553 \quad 0.14775427], \quad (50a)$$

$$\text{eig } \mathbf{B}_{H,N}^{-1} = [0.11659856 \quad 0.12501264 \quad 0.13370292], \quad (50b)$$

for the GaNi scheme (19)

$$\text{eig } \mathbf{A}_{H,N}^{\text{GaNi}} = [0.12635922 \quad 0.13525791 \quad 0.14487843], \quad (51a)$$

$$\text{eig}(\mathbf{B}_{H,N}^{\text{GaNi}})^{-1} = [0.12635914 \quad 0.13525783 \quad 0.14487836], \quad (51b)$$

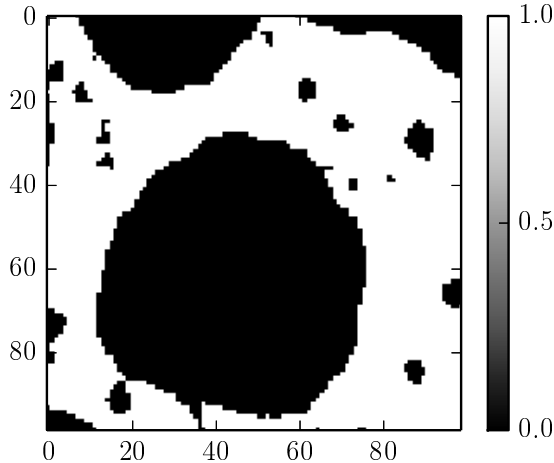


Figure 9: A frontal view on a three-dimensional cell

and for their corresponding guaranteed bounds (20)

$$\text{eig } \tilde{\mathbf{A}}_{\mathbf{H},\mathbf{N}} = [0.13140661 \quad 0.14087040 \quad 0.15016215], \quad (52a)$$

$$\text{eig}(\tilde{\mathbf{B}}_{\mathbf{H},\mathbf{N}}^{-1}) = [0.10289562 \quad 0.11066014 \quad 0.11795426]. \quad (52b)$$

The eigenvalues of the GaNi formulation (51) differ only because of an algebraic error and this confirms the duality of the GaNi scheme stated in [9, Propositin 34] (see Remark 13 for an overview). Moreover, they are located between the guaranteed bounds obtained by both the Ga (50) and the GaNi (52) schemes, and thus the GaNi provides an applicable prediction of homogenized properties. Because the guaranteed bounds comply with the energetic norms of minimizers, the Ga (50) signifies a better approximation of local fields than the GaNi (52). This gap is accentuated in highly-contrasted media.

7 Conclusion

This paper is based on the author’s previous results [21, 9] involving reliable determination of homogenized properties arising from the unit cell problem (15) discretized by trigonometric polynomials [22]. While the previous work [9] dealt with a numerical scheme based on Galerkin approximation with numerical integration (GaNi), fully equivalent to the original Moulinec–Suquet algorithm, this paper is dedicated to Galerkin approximation (Ga) with exact integration. To summarize the most important findings:

- The methodology for efficient double grid quadrature from the author’s previous work [9, section 6] is generalized for material coefficients defined via high-resolution images assuming e.g. piece-wise constant or bilinear fields. See section 4.3 for details.
- Both the Ga (18) and GaNi (19) schemes leads to fully discrete formulations with the very similar block-sparse structure of corresponding linear systems. However, the Ga is primarily evaluated on a double grid resulting in higher computational and memory requirements. See section 5 for details, including discussion about incorporation of the FFT algorithm.
- The Ga scheme (18) outperforms the GaNi (19) in the accuracy of guaranteed bounds on homogenized properties, corresponding also to the energetic norm of the minimizers. The gap between the two schemes is accentuated in highly-contrasted media. Thus, the author recommends using a Ga scheme despite computational demands.

- Evaluation of guaranteed bounds depends on knowing the Fourier coefficients of material properties \mathbf{A} . However, the proper approximation of \mathbf{A} can lead to upper-upper and lower-lower guaranteed bounds, section 4.5.
- The Ga scheme evaluated on a double grid can be recast to the original grid using shifts of DFT (58). This leads to reduced memory requirements while not impacting computational costs when solving linear systems, see section 4.4.
- Contrary to GaNi, the Ga scheme exhibits monotonous behavior, without oscillations in homogenized properties, for an increase in grid points and for a change in inclusion size.
- Both schemes have the same rate of convergence of both minimizers and homogenized properties, which confirms the theoretical results in [22]. From the rate of convergence, it is possible to predict the grid size for a required level of accuracy.
- The Ga scheme can be effectively solved using conjugate gradients providing monotonous improvements of guaranteed bounds during iterations. Moreover, an approximate solution on a coarse grid can be easily transferred to a fine grid to significantly improve the convergence of the solution to the linear system.

A Trigonometric polynomials and their fully discrete counterparts

This section deals with trigonometric polynomials, which are essential for the discretization in section 3.3, for the numerical integration in section 4, and finally for the fully discrete formulations leading to linear systems in section 5. Because of this and for the reader's comfort, the author repeats here the previous results according to [9, section 4], where the trigonometric polynomials were defined in a manner which provided conforming discretization for both the odd (17) and non-odd grids. Here, however, the author omits the fully discrete spaces for the non-odd grids because they are redundant for the Galerkin approximation scheme (18). Please refer to section 4.1 for notation used throughout this appendix.

A.1 Trigonometric polynomials

Definition 43 (Trigonometric polynomials). *For $\mathbf{N} \in \mathbb{N}^d$, approximation and interpolation spaces of \mathbb{R}^d -valued trigonometric polynomials are defined by*

$$\mathcal{T}_{\mathbf{N}}^d = \left\{ \sum_{\mathbf{k} \in \mathring{\mathbb{Z}}_{\mathbf{N}}^d} \hat{\mathbf{v}}^{\mathbf{k}} \varphi_{\mathbf{k}} : \hat{\mathbf{v}}^{\mathbf{k}} = \overline{(\hat{\mathbf{v}}^{-\mathbf{k}})} \in \mathbb{C}^d \right\}, \quad (53a)$$

$$\tilde{\mathcal{T}}_{\mathbf{N}}^d = \left\{ \sum_{\mathbf{k} \in \mathbb{Z}_{\mathbf{N}}^d} \mathbf{v}^{\mathbf{k}} \varphi_{\mathbf{N},\mathbf{k}} : \mathbf{v}^{\mathbf{k}} \in \mathbb{R}^d \right\}, \quad (53b)$$

where reduced and full index sets stand for

$$\mathring{\mathbb{Z}}_{\mathbf{N}}^d = \left\{ \mathbf{k} \in \mathbb{Z}^d : -\frac{N_{\alpha}}{2} < k_{\alpha} < \frac{N_{\alpha}}{2} \right\}, \quad \mathbb{Z}_{\mathbf{N}}^d = \left\{ \mathbf{k} \in \mathbb{Z}^d : -\frac{N_{\alpha}}{2} \leq k_{\alpha} < \frac{N_{\alpha}}{2} \right\}, \quad (54)$$

and the spaces \mathcal{T}_N^d and $\tilde{\mathcal{T}}_N^d$ are spanned by the Fourier and fundamental trigonometric polynomials, respectively:

$$\varphi_{\mathbf{k}}(\mathbf{x}) = \exp\left(2\pi i \sum_{\alpha} \frac{k_{\alpha} x_{\alpha}}{Y_{\alpha}}\right), \quad (55a)$$

$$\varphi_{N,\mathbf{k}}(\mathbf{x}) = \frac{1}{|N|} \sum_{\mathbf{m} \in \mathbb{Z}_N^d} \omega_N^{-\mathbf{k}\mathbf{m}} \varphi_{\mathbf{m}}(\mathbf{x}), \quad (55b)$$

with the coefficients

$$\omega_N^{\mathbf{k}\mathbf{m}} = \exp\left(2\pi i \sum_{\alpha} \frac{k_{\alpha} m_{\alpha}}{N_{\alpha}}\right) \quad \text{for } \mathbf{k}, \mathbf{m} \in \mathbb{Z}^d.$$

The remainder of this section is devoted to clarifying the connection between the two definitions of trigonometric polynomials (53), index sets (54), and basis functions (55).

The *approximation space* \mathcal{T}_N^d provides a finite-dimensional subspace to $L_{\#}^2(\mathcal{Y}; \mathbb{R}^d)$ for the Galerkin method. Its conformity, i.e. $\mathcal{T}_N^d \subset L_{\#}^2(\mathcal{Y}; \mathbb{R}^d)$, is ensured once the Hermitian symmetry of the Fourier coefficients holds, compare (53a) with (7). This condition is easily enforced for odd grids which are symmetric with respect to the origin, Figure 10(a). For non-odd grids, the highest (Nyquist) frequencies $k_{\alpha} = -N_{\alpha}/2$ must be omitted, leading to the notion of the reduced index set $\tilde{\mathbb{Z}}_N^d$.

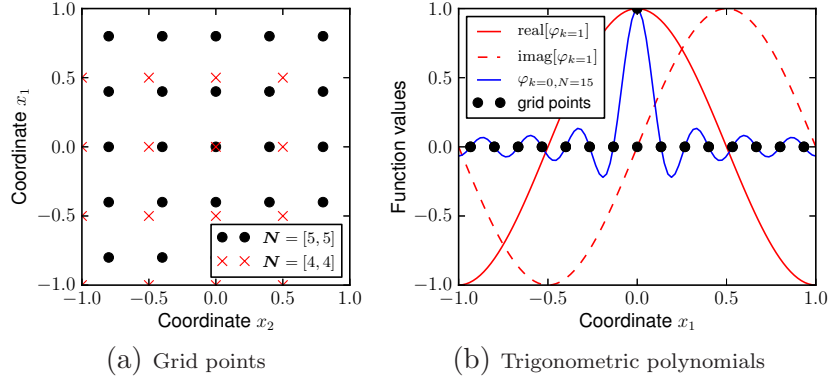


Figure 10: Two-dimensional grids points (56) and one-dimensional basis trigonometric polynomials (55)

The *interpolation space* $\tilde{\mathcal{T}}_N^d$ will be used to perform the numerical quadrature with the Galerkin method and primarily works with real data instead of the Fourier domain. Its connection to the approximation space is established with the Discrete Fourier Transform (DFT) and its inverse (iDFT)

$$\hat{\mathbf{u}}_N(\mathbf{k}) = \frac{1}{|N|} \sum_{\mathbf{m} \in \mathbb{Z}_N^d} \omega_N^{-\mathbf{k}\mathbf{m}} \mathbf{u}_N(\mathbf{x}_N^{\mathbf{m}}), \quad \mathbf{u}_N(\mathbf{x}_N^{\mathbf{k}}) = \sum_{\mathbf{m} \in \mathbb{Z}_N^d} \omega_N^{\mathbf{k}\mathbf{m}} \hat{\mathbf{u}}_N(\mathbf{m}) \quad \text{for } \mathbf{k} \in \mathbb{Z}_N^d,$$

where an orthogonality relation is utilized

$$\sum_{\mathbf{n} \in \mathbb{Z}_N^d} \omega_N^{-\mathbf{k}\mathbf{n}} \omega_N^{\mathbf{n}\mathbf{m}} = |N| \delta_{\mathbf{k}\mathbf{m}} \quad \text{for } \mathbf{k}, \mathbf{m} \in \mathbb{Z}_N^d,$$

and by $\mathbf{x}_N^{\mathbf{k}}$ the author denoted the grid points

$$\mathbf{x}_N^{\mathbf{k}} = \sum_{\alpha} \frac{Y_{\alpha} k_{\alpha}}{N_{\alpha}} \mathbf{U}^{(\alpha)} \quad \text{for } \mathbf{k} \in \mathbb{Z}_N^d. \quad (56)$$

Indeed, expanding a function $\mathbf{u}_N : \mathcal{Y} \rightarrow \mathbb{C}^d$ into the Fourier series

$$\begin{aligned} \mathbf{u}_N(\mathbf{x}) &= \sum_{\mathbf{k} \in \mathbb{Z}_N^d} \hat{\mathbf{u}}_N(\mathbf{k}) \varphi_{\mathbf{k}}(\mathbf{x}) = \frac{1}{|\mathbb{N}|} \sum_{\mathbf{k} \in \mathbb{Z}_N^d} \sum_{\mathbf{m} \in \mathbb{Z}_N^d} \omega_N^{-\mathbf{k}\mathbf{m}} \mathbf{u}_N(\mathbf{x}_N^{\mathbf{m}}) \varphi_{\mathbf{k}}(\mathbf{x}) \\ &= \sum_{\mathbf{m} \in \mathbb{Z}_N^d} \underbrace{\sum_{\mathbf{k} \in \mathbb{Z}_N^d} \frac{1}{|\mathbb{N}|} \omega_N^{-\mathbf{k}\mathbf{m}} \varphi_{\mathbf{k}}(\mathbf{x}) \mathbf{u}_N(\mathbf{x}_N^{\mathbf{m}})}_{\varphi_{N,\mathbf{m}}(\mathbf{x})} \end{aligned}$$

gives rise to the fundamental trigonometric polynomial $\varphi_{N,\mathbf{m}}$. In addition, these basis functions possess the Dirac delta property, $\varphi_{N,\mathbf{k}}(\mathbf{x}_N^{\mathbf{m}}) = \delta_{\mathbf{k}\mathbf{m}}$, Figure 10(b).

For further reference, these relations can be represented in compact by

$$\mathbf{u}_N = \sum_{\mathbf{k} \in \mathbb{Z}_N^d} \hat{\mathbf{u}}_N^{\mathbf{k}} \varphi_{\mathbf{k}} = \sum_{\mathbf{k} \in \mathbb{Z}_N^d} \mathbf{u}_N^{\mathbf{k}} \varphi_{N,\mathbf{k}} \quad \text{with } \hat{\mathbf{u}}_N = \mathbf{F}_N \mathbf{u}_N \in \mathbb{C}^{d \times N}, \quad (57)$$

where $\hat{\mathbf{u}}_N^{\mathbf{k}} = \hat{\mathbf{u}}_N(\mathbf{k}) \in \mathbb{C}^d$ and $\mathbf{u}_N^{\mathbf{k}} = \mathbf{u}_N(\mathbf{x}_N^{\mathbf{k}}) \in \mathbb{C}^d$, and the matrices

$$\mathbf{F}_N = \frac{1}{|\mathbb{N}|} (\delta_{\alpha\beta} \omega_N^{-\mathbf{m}\mathbf{k}})_{\alpha,\beta}^{\mathbf{m},\mathbf{k} \in \mathbb{Z}_N^d} \in [\mathbb{C}^{d \times N}]^2, \quad \mathbf{F}_N^{-1} = (\delta_{\alpha\beta} \omega_N^{\mathbf{m}\mathbf{k}})_{\alpha,\beta}^{\mathbf{m},\mathbf{k} \in \mathbb{Z}_N^d} \in [\mathbb{C}^{d \times N}]^2 \quad (58)$$

implement the vector-valued DFT and iDFT.

The relation between the two spaces of trigonometric polynomials depends on grid parity. For odd grids, $\mathbb{Z}_N^d \setminus \mathring{\mathbb{Z}}_N^d = \emptyset$, and it follows from (57) that the spaces coincide:

$$\mathcal{T}_N^d = \tilde{\mathcal{T}}_N^d, \quad \mathring{\mathbb{Z}}_N^d = \mathbb{Z}_N^d \quad \text{for odd grid assumption (17).}$$

This property is lost in general due to the Nyquist frequencies $\mathbf{k} \in \mathbb{Z}_N^d \setminus \mathring{\mathbb{Z}}_N^d$, and only the following inclusions hold

$$\mathcal{T}_N^d \subseteq \tilde{\mathcal{T}}_N^d, \quad \mathring{\mathbb{Z}}_N^d \subseteq \mathbb{Z}_N^d.$$

As a result, the interpolation space is non-conforming for non-odd grids, $\tilde{\mathcal{T}}_N^d \not\subset L_{\#}^2(\mathcal{Y}; \mathbb{R}^d)$, because the fundamental trigonometric polynomials (55b) become complex-valued off the grids points, despite being real-valued at the grid points due to the Dirac delta property. Thus, the interpolation space $\tilde{\mathcal{T}}_N^d$ admits an equivalent definition via Fourier coefficients

$$\tilde{\mathcal{T}}_N^d = \left\{ \sum_{\mathbf{k} \in \mathbb{Z}_N^d} \hat{\mathbf{v}}_N^{\mathbf{k}} \varphi_{\mathbf{k}} : \hat{\mathbf{v}}_N \in \mathbf{F}_N(\mathbb{R}^{d \times N}) \right\}.$$

These arguments can be formalized by introducing suitable operators, which will be useful when dealing with the Galerkin approximations and their fully discrete versions in sections 3.3 and 5.

Definition 44 (Operators). *Using grid points $\mathbf{x}_N^{\mathbf{k}}$ for $\mathbf{N} \in \mathbb{N}^d$ and $\mathbf{k} \in \mathbb{Z}_N^d$ according to (56), the interpolation operator $\mathcal{Q}_N : C_{\#}(\mathcal{Y}; \mathbb{R}^d) \rightarrow L_{\#}^2(\mathcal{Y}; \mathbb{C}^d)$, the truncation operator $\mathcal{P}_N : L_{\#}^2(\mathcal{Y}; \mathbb{R}^d) \rightarrow L_{\#}^2(\mathcal{Y}; \mathbb{R}^d)$, and the discretization operator $\mathcal{I}_N : C_{\#}^0(\mathcal{Y}; \mathbb{C}^d) \rightarrow \mathbb{C}^{d \times N}$, are defined by*

$$\mathcal{Q}_N[\mathbf{u}] = \sum_{\mathbf{k} \in \mathbb{Z}_N^d} \mathbf{u}(\mathbf{x}_N^{\mathbf{k}}) \varphi_{N,\mathbf{k}}, \quad \mathcal{P}_N[\mathbf{u}] = \sum_{\mathbf{k} \in \mathring{\mathbb{Z}}_N^d} \hat{\mathbf{u}}(\mathbf{k}) \varphi_{\mathbf{k}}, \quad \mathcal{I}_N[\mathbf{u}] = (u_{\alpha}(\mathbf{x}_N^{\mathbf{k}}))_{\alpha=1,\dots,d}^{\mathbf{k} \in \mathbb{Z}_N^d}. \quad (59)$$

The following lemma summarizes the relevant properties of operators (59) and trigonometric polynomials (55). The proof generalizes the results from [30, 21, 22] obtained under the odd grid assumption (17) to a general case; it is outlined here to keep the paper self-contained.

Lemma 45. (i) For $\mathbf{k}, \mathbf{m} \in \mathbb{Z}_N^d$, it holds

$$\varphi_{\mathbf{k}}(\mathbf{x}_N^{\mathbf{m}}) = \omega_N^{\mathbf{k}\mathbf{m}}, \quad (60a)$$

$$\varphi_{N,\mathbf{k}}(\mathbf{x}_N^{\mathbf{m}}) = \delta_{\mathbf{k}\mathbf{m}}, \quad (60b)$$

$$(\varphi_{N,\mathbf{k}}, \varphi_{N,\mathbf{m}})_{L^2_{\#}(\mathcal{Y})} = \frac{\delta_{\mathbf{k}\mathbf{m}}}{|N|}. \quad (60c)$$

(ii) The operator \mathcal{I}_N is an one-to-one isometric map from $\tilde{\mathcal{T}}_N^d$ onto $\mathbb{R}^{d \times N}$, i.e. for all $\mathbf{u}_N, \mathbf{v}_N \in \tilde{\mathcal{T}}_N^d$

$$(\mathbf{u}_N, \mathbf{v}_N)_{L^2_{\#}(\mathcal{Y}; \mathbb{R}^d)} = (\mathcal{I}_N[\mathbf{u}_N], \mathcal{I}_N[\mathbf{v}_N])_{\mathbb{R}^{d \times N}}.$$

Moreover, for all $\mathbf{u} \in C^0_{\#}(\mathcal{Y}; \mathbb{R}^d)$, it holds

$$\mathcal{I}_N[\mathcal{Q}_N[\mathbf{u}]] = \mathcal{I}_N[\mathbf{u}].$$

(iii) The interpolation operator \mathcal{Q}_N is a projection with image $\tilde{\mathcal{T}}_N^d$,

(iv) The truncation operator \mathcal{P}_N is an orthogonal projection with the image \mathcal{T}_N^d .

A.2 Fully discrete spaces — odd grids

The focus of this section is on the fully discrete spaces storing the values of the trigonometric polynomials on grids with an odd number of points (17). As first recognized in [22], the remarkable property of such discretization is that the structure of the continuous problem is translated into the discrete case in a conforming way, cf. Figure 11.

Definition 46 (Fully discrete projections). Let $\hat{\Gamma}^{\bullet}(\mathbf{k}) \in \mathbb{R}^{d \times d}$ for $\bullet \in \{\mathcal{U}, \mathcal{E}, \mathcal{J}\}$ and $\mathbf{k} \in \mathbb{Z}^d$ be the Fourier coefficients from Definition 1. Assuming odd grids (17), the author defines block diagonal matrices $\hat{\mathbf{G}}_N^{\mathcal{U}}, \hat{\mathbf{G}}_N^{\mathcal{E}}$, and $\hat{\mathbf{G}}_N^{\mathcal{J}} \in [\mathbb{R}^{d \times N}]^2$ in the Fourier domain as

$$(\hat{\mathbf{G}}_N^{\bullet})_{\alpha\beta}^{\mathbf{k}\mathbf{m}} = \hat{\Gamma}_{\alpha\beta}^{\bullet}(\mathbf{k})\delta_{\mathbf{k}\mathbf{m}}, \quad (61)$$

where $\mathbf{k}, \mathbf{m} \in \mathbb{Z}_N^d$ and $\bullet \in \{\mathcal{U}, \mathcal{E}, \mathcal{J}\}$. The real domain equivalents are obtained with similarity transformations using DFT (58), i.e.

$$\mathbf{G}_N^{\bullet} = \mathbf{F}_N^{-1} \hat{\mathbf{G}}_N^{\bullet} \mathbf{F}_N.$$

Lemma 47. Matrices \mathbf{G}_N^{\bullet} for $\bullet \in \{\mathcal{U}, \mathcal{E}, \mathcal{J}\}$ constitute the identity

$$\mathbf{G}_N^{\mathcal{U}} + \mathbf{G}_N^{\mathcal{E}} + \mathbf{G}_N^{\mathcal{J}} = \mathbf{I}$$

and are mutually orthogonal projections on $\mathbb{R}^{d \times N}$.

Definition 48 (Finite dimensional subspaces). The previously defined projections provide us with the following subspaces of $\mathbb{R}^{d \times N}$

$$\mathbf{U}_N = \mathbf{G}_N^{\mathcal{U}}[\mathbb{R}^{d \times N}], \quad \mathbf{E}_N = \mathbf{G}_N^{\mathcal{E}}[\mathbb{R}^{d \times N}], \quad \mathbf{J}_N = \mathbf{G}_N^{\mathcal{J}}[\mathbb{R}^{d \times N}], \quad (62)$$

and their trigonometric counterparts

$$\mathcal{U}_N = \mathcal{I}_N^{-1}[\mathbf{U}_N], \quad \mathcal{E}_N = \mathcal{I}_N^{-1}[\mathbf{E}_N], \quad \mathcal{J}_N = \mathcal{I}_N^{-1}[\mathbf{J}_N].$$

$$\begin{array}{rcl}
L^2_{\text{per}}(\mathcal{Y}; \mathbb{R}^d) \supset & \mathcal{T}_N^d & = \mathcal{I}_N^{-1}[\mathbb{R}^{d \times N}] \\
\parallel & \parallel & \parallel \\
\mathcal{U} = & \mathcal{U} & = \mathcal{I}_N^{-1}[\mathbb{U}_N] \\
\oplus^\perp & \oplus^\perp & \oplus^\perp \\
\mathcal{E} \supset & \mathcal{E}_N & = \mathcal{I}_N^{-1}[\mathbb{E}_N] \\
\oplus^\perp & \oplus^\perp & \oplus^\perp \\
\mathcal{J} \supset & \mathcal{J}_N & = \mathcal{I}_N^{-1}[\mathbb{J}_N]
\end{array}$$

Figure 11: The scheme of subspaces for odd grids

The relation of these subspaces to the Helmholtz decomposition (11) is clarified by Figure 11 and the following lemma.

Lemma 49. (i) Space $\mathbb{R}^{d \times N}$ can be decomposed into three mutually orthogonal subspaces

$$\mathbb{R}^{d \times N} = \mathbb{U}_N \oplus \mathbb{E}_N \oplus \mathbb{J}_N.$$

(ii) The scheme in Figure 11 is valid and

$$\mathcal{G}^\bullet[\mathcal{T}_N^d] = \mathcal{I}_N^{-1}[\mathbf{G}^\bullet_N[\mathbb{R}^{d \times N}]] \quad \text{for } \bullet \in \{\mathcal{U}, \mathcal{E}, \mathcal{J}\}.$$

Remark 50. The previous proof yields an alternative characterization of the conforming subspaces

$$\mathcal{U}_N = \mathcal{U} \cap \mathcal{T}_N^d, \quad \mathcal{E}_N = \mathcal{E} \cap \mathcal{T}_N^d, \quad \mathcal{J}_N = \mathcal{J} \cap \mathcal{T}_N^d.$$

Acknowledgement

This work has been supported by project EXLIZ – CZ.1.07/2.3.00/30.0013 which is co-financed by the European Social Fund and the national budget of the Czech Republic and by the Czech Science Foundation through project No. P105/12/0331.

References

- [1] Flaherty JE, Keller JB. Elastic behavior of composite media. *Communications on Pure and Applied Mathematics* 1973; **26**(4):565–580, doi:10.1002/cpa.3160260409.
- [2] Garboczi E. Finite element and finite difference programs for computing the linear electric and elastic properties of digital images of random materials. *Technical Report NISTIR 6269*, Building and Fire Research Laboratory, National Institute of Standards and Technology, Gaithersburg, Maryland 2089 1998. URL <http://fire.nist.gov/bfrlpubs/build98/art147.html>.
- [3] Guedes J, Kikuchi N. Preprocessing and postprocessing for materials based on the homogenization method with adaptive finite element methods. *Computer Methods in Applied Mechanics and Engineering* 1990; **83**(2):143–198, doi:10.1016/0045-7825(90)90148-F.
- [4] Geers M, Kouznetsova V, Brekelmans W. Multi-scale computational homogenization: Trends and challenges. *Journal of Computational and Applied Mathematics* 2010; **234**(7):2175–2182, doi:10.1016/j.cam.2009.08.077.
- [5] Eischen J, Torquato S. Determining elastic behavior of composites by the boundary element method. *Journal of applied physics* 1993; **74**(1):159–170.

- [6] Procházka P, Šejnoha J. A BEM formulation for homogenization of composites with randomly distributed fibers. *Engineering analysis with boundary elements* 2003; **27**(2):137–144.
- [7] Greengard L, Lee J. Electrostatics and heat conduction in high contrast composite materials. *Journal of Computational Physics* 2006; **211**(1):64–76.
- [8] Helsing J. The effective conductivity of arrays of squares: large random unit cells and extreme contrast ratios. *Journal of Computational Physics* 2011; **230**(20):7533–7547.
- [9] Vondřejc J, Zeman J, Marek I. Guaranteed upper-lower bounds on homogenized properties by FFT-based Galerkin method. *arXiv:1404.3614* 2014; URL <http://arxiv.org/abs/1404.3614>.
- [10] Kabel M, Böhlke T, Schneider M. Efficient fixed point and Newton-Krylov solvers for FFT-based homogenization of elasticity at large deformations. *Computational Mechanics* 2014; doi:10.1007/s00466-014-1071-8.
- [11] Šmilauer V, Bažant ZP. Identification of viscoelastic C-S-H behavior in mature cement paste by FFT-based homogenization method. *Cement and Concrete Research* 2010; **40**(2):197–207.
- [12] Vinogradov V, Milton GW. An accelerated FFT algorithm for thermoelastic and non-linear composites. *International Journal for Numerical Methods in Engineering* 2008; **76**(11):1678–1695, doi:10.1002/nme.
- [13] Li J, Meng S, Tian X, Song F, Jiang C. A non-local fracture model for composite laminates and numerical simulations by using the FFT method. *Composites Part B: Engineering* 2012; **43**(3):961–971, doi:10.1016/j.compositesb.2011.08.055.
- [14] Li J, Tian X, Abdelmoula R. A damage model for crack prediction in brittle and quasi-brittle materials solved by the FFT method. *International Journal of Fracture* 2012; **173**(2):135–146, doi:10.1007/s10704-011-9671-1.
- [15] Papanicolau G, Bensoussan A, Lions J. *Asymptotic analysis for periodic structures*, vol. 5. North Holland, 1978.
- [16] Jikov VV, Kozlov SM, Oleinik OA. *Homogenization of Differential Operators and Integral Functionals*. Springer-Verlag, 1994.
- [17] Cioranescu D, Donato P. *An Introduction to Homogenization*. Oxford Lecture Series in Mathematics and Its Applications, Oxford University Press, 1999.
- [18] Moulinec H, Suquet P. A fast numerical method for computing the linear and nonlinear mechanical properties of composites. *Comptes rendus de l'Académie des sciences. Série II, Mécanique, physique, chimie, astronomie* 1994; **318**(11):1417–1423.
- [19] Brisard S, Dormieux L. FFT-based methods for the mechanics of composites: A general variational framework. *Computational Materials Science* 2010; **49**(3):663–671.
- [20] Brisard S, Dormieux L. Combining Galerkin approximation techniques with the principle of Hashin and Shtrikman to derive a new FFT-based numerical method for the homogenization of composites. *Computer Methods in Applied Mechanics and Engineering* 2012; **217-220**:197–212, doi:10.1016/j.cma.2012.01.003.
- [21] Vondřejc J. FFT-based method for homogenization of periodic media: Theory and applications. PhD Thesis, Czech Technical University in Prague 2013. URL http://mech.fsv.cvut.cz/wiki/images/4/49/PhD_dissertation_Vondrej_c_2013.pdf.

- [22] Vondřejc J, Zeman J, Marek I. An FFT-based Galerkin method for homogenization of periodic media. *Computers and Mathematics with Applications* 2014; **68**(3):156–173, doi:10.1016/j.camwa.2014.05.014.
- [23] Vondřejc J, Zeman J, Marek I. Analysis of a Fast Fourier Transform Based Method for Modeling of Heterogeneous Materials. *Lecture Notes in Computer Science* 2012; **7116**:512–522.
- [24] Nemat-Nasser S, Yu N, Hori M. Bounds and estimates of overall moduli of composites with periodic microstructure. *Mechanics of Materials* 1993; **15**(3):163–181, doi:10.1016/0167-6636(93)90016-K.
- [25] Luciano R, Sacco E. Variational methods for the homogenization of periodic heterogeneous media. *European Journal of Mechanics - A/Solids* 1998; **17**(4):599–617, doi:10.1016/S0997-7538(99)80024-2.
- [26] Cai H, Xu Y. A Fast Fourier-Galerkin Method for Solving Singular Boundary Integral Equations. *SIAM Journal on Numerical Analysis* 2008; **46**(4):1965–1984, doi:10.1137/070703478.
- [27] Næss OF, Eckhoff KS. A Modified Fourier-Galerkin Method for the Poisson and Helmholtz Equations. *Journal of Scientific Computing* 2002; **17**(1-4):529–539, doi:10.1023/A:1015162328151.
- [28] Zeman J, Vondřejc J, Novák J, Marek I. Accelerating a FFT-based solver for numerical homogenization of periodic media by conjugate gradients. *Journal of Computational Physics* 2010; **229**(21):8065–8071, doi:10.1016/j.jcp.2010.07.010.
- [29] Vainikko G. Fast solvers of the Lippmann-Schwinger equation. *Direct and Inverse Problems of Mathematical Physics* 2000; **5**:423–440.
- [30] Saranen J, Vainikko G. *Periodic Integral and Pseudodifferential Equations with Numerical Approximation*. Springer Monographs Mathematics: Berlin, Heidelberg, 2002.
- [31] Moulinec H, Suquet P. A numerical method for computing the overall response of nonlinear composites with complex microstructure. *Computer Methods in Applied Mechanics and Engineering* 1997; **157**(1–2):69–94, doi:10.1016/S0045-7825(97)00218-1.
- [32] Bonnet G. Effective properties of elastic periodic composite media with fibers. *Journal of the Mechanics and Physics of Solids* 2007; **55**(5):881–899, doi:10.1016/j.jmps.2006.11.007.
- [33] Monchiet V, Bonnet G. A polarization-based FFT iterative scheme for computing the effective properties of elastic composites with arbitrary contrast. *International Journal for Numerical Methods in Engineering* 2012; **89**(11):1419–1436, doi:10.1002/nme.3295.
- [34] Michel J, Moulinec H, Suquet P. A computational method based on augmented Lagrangians and fast Fourier transforms for composites with high contrast. *CMES: Computer Modeling in Engineering & Sciences* 2000; **1**(2):79–88.
- [35] Willot F, Abdallah B, Pellegrini YP. Fourier-based schemes with modified Green operator for computing the electrical response of heterogeneous media with accurate local fields. *International Journal for Numerical Methods in Engineering* 2014; **98**(7):518–533, doi:10.1002/nme.4641.
- [36] Craster RV, Obnosov YV. Four-phase checkerboard composites. *SIAM Journal on Applied Mathematics* 2001; **61**(6):1839–1856.

- [37] Eyre DJ, Milton GW. A fast numerical scheme for computing the response of composites using grid refinement. *The European Physical Journal Applied Physics* 1999; **6**(1):41–47.
- [38] Voigt W. *Lehrbuch der kristallphysik*, vol. 34. BG Teubner, 1910.
- [39] Reuss A. Berechnung der Fließgrenze von Mischkristallen auf Grund der Plastizitätsbedingung für Einkristalle. *ZAMM-Journal of Applied Mathematics and Mechanics/Zeitschrift für Angewandte Mathematik und Mechanik* 1929; **9**(1):49–58.
- [40] Hashin Z, Shtrikman S. A variational approach to the theory of the elastic behaviour of multiphase materials. *Journal of the Mechanics and Physics of Solids* 1963; **11**(2):127–140.
- [41] Milton GW. *The Theory of Composites, Cambridge Monographs on Applied and Computational Mathematics*, vol. 6. Cambridge University Press: Cambridge, UK, 2002.
- [42] Torquato S. *Random heterogeneous materials: microstructure and macroscopic properties*, vol. 16. Springer, 2002.
- [43] Cherkhaev A. *Variational methods for structural optimization*, vol. 140. Springer, 2000.
- [44] Dvorak GJ. *Micromechanics of Composite Materials*, vol. 186. Springer, 2012.
- [45] Dvořák J. Optimization of Composite Materials. Master’s Thesis, Charles University 1993.
- [46] Haslinger J, Dvořák J. Optimum composite material design. *RAIRO-Mathematical Modelling and Numerical Analysis-Modelisation Mathématique et Analyse Numérique* 1995; **29**(6):657–686.
- [47] Wieckowski Z. Dual Finite Element Methods in Mechanics of Composite Materials. *Journal of Theoretical and Applied Mechanics* 1995; **2**(33):233–252.
- [48] Kabel M, Andrä H. Fast numerical computation of precise bounds of effective elastic moduli. 2012; URL http://math2market.de/Publications/2013ReportFraunhoferITWM_Nr224.pdf.
- [49] Bignonnet F, Dormieux L. FFT-based bounds on the permeability of complex microstructures. *International Journal for Numerical and Analytical Methods in Geomechanics* 2014; **38**(16):1707–1723, doi:10.1002/nag.2278.
- [50] Schneider M. Convergence of FFT-based homogenization for strongly heterogeneous media. *Mathematical Methods in the Applied Sciences* 2014; doi:10.1002/mma.3259.
- [51] Monchiet V. Combining FFT methods and standard variational principles to compute bounds and estimates for the properties of elastic composites. *Computer Methods in Applied Mechanics and Engineering* 2015; **283**:454–473, doi:10.1016/j.cma.2014.10.005.
- [52] Horn RA, Johnson CR. *Matrix analysis*. Second edn., Cambridge University Press: 32 Avenue of the Americas, New York, NY 10013-2473, USA, 2013.
- [53] Rudin W. *Real and complex analysis*. third edn., McGraw-Hill: New York, 1986.
- [54] Ekeland I, Temam R. *Convex Analysis and Variational Problems*. SIAM, 1976.
- [55] Suquet P. Une méthode duale en homogénéisation: application aux milieux élastiques. *Journal de Mécanique théorique et Appliquée (Special issue)* 1982; :79–98.
- [56] Trefethen LN, Bau D. *Numerical linear algebra*. Society for Industrial Mathematics, 1997.

- [57] Saad Y. *Iterative Methods for Sparse Linear Systems*. Second edn., Society for Industrial and Applied Mathematics: Philadelphia, PA, USA, 2003.
- [58] Strang G. Variational crimes in the finite element method. *The mathematical foundations of the finite element method with applications to partial differential equations* 1972; :689–710.
- [59] Hlaváček P, Šmilauer V, Škvára F, Kopecký L, Šulc R. Inorganic foams made from alkali-activated fly ash: Mechanical, chemical and physical properties. *Journal of the European Ceramic Society* 2015; **35**(2):703–709, doi:10.1016/j.jeurceramsoc.2014.08.024.